

**Ministry of Higher Education and Scientific Research  
University of Baghdad  
Institute of Laser for Postgraduate Studies**



# **Design and Implementation of Multimode Fiber Mach Zehnder Interferometer for Sensor Network**

**A Thesis Submitted to the Institute of Laser for Postgraduate Studies,  
University of Baghdad in Partial Fulfillment of the Requirements for the  
degree of Master of Science in Laser/ Electronic and Communication  
Engineering**

**By**

**Asmaa Anaam Abdulwahhab**

**B.Sc. Electronics and Communication Engineering – 2013**

**Supervisor**

**Asst. Prof. Dr. Tahreer Safa'a Mansour**

**2021 AD**

**1443AH**

بِسْمِ اللَّهِ الرَّحْمَنِ الرَّحِيمِ

وَاللَّهُ يَوْمَئِذٍ عَلِيمٌ  
رَبِّكَ الْكَافِرُ  
سَنَةَ بَيْتِ  
دَاوُدَ

بِعْرَافٍ (٤٧)

ضُرُوقِ اللَّهِ الْعَظِيمِ

سورة الحج اية (٤٧)

## إلى من قدر عليه مفارقتي باكرا في هذه الحياة ، لتبقى روحه حاضرتنا ، ويحيا في شغافي ما حييت ، إلى من شاركني أحلام نجاحي معتزا بي ولم يشأ القدر ان يكون حاضري الحظة ، إلى روح والدي الشهيد الحبيب

إلى معلم الأمة والشفيع المرتجي حبيب الله سيدنا محمد خاتم الانبياء والمرسلين (صلى الله عليه وعلى اله وصحبه الغر الميامين وسلم تسليما كثيرا )

إلى من قدر عليه مفارقتي باكرا في هذه الحياة ، لتبقى روحه حاضرتنا ، ويحيا في شغافي ما حييت ، إلى من شاركني أحلام نجاحي معتزا بي ولم يشأ القدر ان يكون حاضري الحظة ، إلى روح والدي الشهيد الحبيب  
رحمه الله

إلى مصدر قوتي وشريكة نجاحي وواعظم نعم الله علي وطريق جنتي ، إلى من تزرع الأمل في  
طريقي دوماً بمناجاتها ودعواتها والدي جوف فؤادي حفظها الله.

إلى أخوتي اللذين وهبهم الله لي سببا لعونه لي وفقهم الله.

إلى اخواتي اللواتي انعم الله بهن عليّة لتم سعادتي العزيزات على قلبي اسعدهم الله

إلى وطني الجريح اغاثك الله رب العالمين

إلى شهداء وطني المظلومين رحمهم الله

اهدي ثمرة جهدي هذه

إلى من قدر عليه مفارقتي باكرا في هذه الحياة ، لتبقى روحه حاضرتنا ، ويحيا في شغافي ما حييت ، إلى من شاركني أحلام نجاحي معتزا بي ولم يشأ القدر ان يكون حاضري الحظة ، إلى روح والدي الشهيد الحبيب

## Acknowledgement

I'm so honored to have this opportunity to thank all the people who have helped me over the past two years.

Firstly, I thank "ALLAH ALMIGHTY" for guiding and retaining me during my whole life. I would like sincerely thank to supervisor, Ass. Prof. Dr Tahreer Safa'a Mansor, (head of the Engineering and Industrial Applications Department and my supervisor ), for his guidance in every aspect of this thesis. She has allowed me to choose and direct my own project. She has given me a wealth of experience and professional confidence, which is arguably the most valuable inheritance from a graduate degree.

I would like to thank **Prof. Dr. Hussein Ali Jawad**,, the Dean of Institute of Laser for Postgraduate Studies and all the staff of the Institute for their effort during this research work. Special thanks are to **Dr. Jawad A. Hasan**, Asst. Dean of the Institute of Laser for Postgraduate Studies . Many thanks go to all the faculty members and staff of Institute of Laser for Postgraduate Studies, University of Baghdad, especially to **Asst. Prof. Mohammed K. Dhahir**. Great appreciation to **Asst. Prof. Dr. Shelan Khasro Tawfeeq**, for her encouragement Special gratitude to **M.Sc. Nada F. Noori** who gave me great assistances to complete this work.

Finally, my words are unable to express my real happiness to my family especially my father and my husband for their patience and assistance.

*Asmaa Anaam*

## Abstract

Rapid detection is one of the most important process that can be gotten from full width at half maximum (FWHM<sub>spatially</sub>). For the future it could be used in many advanced optical communication systems for high data rate applications.

In this work inline fiber interferometer as a rapid reusable detection system was designed using etched multimode Mach Zehnder fiber interferometer as in line nested configurations.

Two simulators were used to implement the detection system. The etched multimode fiber, and sensing head, were designed with different thicknesses and different surrounding media using Opt grating Version (4.2.2).

The performance of the designed system was investigated practically using pulsed diode laser operating in C-band centered at 1546.74nm, with 10ns pulse width and 1.23 mW peak power. The designed system was used for both chemical and biological applications. First for chemical application, two organic materials ( $C_2H_5OH$ ) and acetone ( $CH_3COCH_3$ ) in addition to distilled water are utilized. The FWHM was 196 pm for distilled water at fiber diameter of 112.9  $\mu m$ , 292 pm for ethanol at fiber diameter of 118.7  $\mu m$  and 365 pm for acetone at fiber diameter of 112.9  $\mu m$ . For biological applications, three samples of pregnant urine (preg 1, preg2, preg3) compared with non-pregnant urine sample were investigated to ability of the designed interferometer for pregnancy test. The FWHM was 243 pm for non-pregnant at fiber diameter 112.9  $\mu m$ , 147 pm for preg1 at fiber diameter 72.5  $\mu m$ , 317 pm for preg2 at fiber diameter 112.9  $\mu m$  and 237 pm for preg3 at fiber diameter 118.7 pm.

In conclusion rapid detection was obtained in the case of nested at minimum full width at half maximum FWHM of 209 pm, central wavelength 1547.2 nm and peak power 66.7  $\mu W$ . In biological applications, rapid full width at half maximum FWHM was detected with 333 pm at central wavelength 1546.85 nm and peak power 7.66  $\mu W$  in case of preg3.

<b>List of Contents</b>		<b>page No.</b>
Abstract		I
List of Contents		Ii
List of Abbreviations		V
List of Symbols		Vi
List of Tables		Vi
List of Figures		Vii
<b>Chapter One: Introduction and basic concept</b>		
1.1	General Introduction and Motivation	1
1.2	The aim of the work	2
1.3	Multimode Fiber (MMF)	3
1.4	In Line Fiber Interferometers	4
	1.4.1 In Line Fabry-Perot Interferometer	4
	1.4.2 In Line Michelson Interferometer	6
	1.4.3 In Lin Sagnac Interferometer	6
	1.4.4 In Line Mach Zehnder Interferometer	7
1.5	Principles of Nested Mach-Zehnder Interferometer	9
	1.5.1 NMZI based on double clad multimode fiber	11
1.6	The Degradation of Signals in Optical Fiber	12
	1.6.1 Transmission loss (attenuation)	13
	1.6.2 Dispersion	14
	1.6.2.1 Chromatic Dispersion	14
	1.6.2.2 Intermodal Dispersion	15
	1.6.2.3 Polarization Mode Dispersion	16
	1.6.3 Nonlinear phenomena	17
	1.6.3.1 Intensity-Dependent Refractive Index	17
	1.6.3.2 Self-Phase Modulation	18
	1.6.3.3 Stimulated Raman scattering	18
	1.6.3.4 Effective length	19

	1.6.4	Nonlinearities phenomena in MMF – MZI	19
1.7	Literature survey		21

<b>Chapter Two : Simulation and Experimental Setup</b>				
	Introduction		26	
2.1	Simulation work		27	
	2.1.1	Etched Multimode fiber using opt grating Design Nested	27	
	2.1.2	Mach-Zehnder interferometer using opt wave	28	
2.2	Experimental work		29	
	2.2.1	The Optical Laser Source	30	
	2.2.2	Erbium Doped Amplifier (EDFA)	31	
	2.2.3	Optical couplers	31	
	2.2.4	Etced MMF-MZ Interferometer	32	
		2.2.4.1	Multimode fiber (MMF)	32
		2.2.4.2	Etching process of MMF	33
	2.2.5	Optical spectrum visualizer ( FBGA Interrogator (OSA))	35	
	2.2.6	Power Meter	36	
	2.2.7	Chemical liquids	36	
		2.2.7.1	Distilled Water	36
		2.2.7.2	Ethanol	37
		2.2.7.3	Acetone	38
	2.2.8	Refractive Index Measurement for Biological Samples	39	
<b>Chapter Three : Results, Discussion and Future Work</b>				

	Introduction	41
3.1	Simulation work	42
	3.1.1 Simulation results of design etched MMF	42
	3.1.2 Simulation results of nested etched MMF -MZI	44
3.2	Experimental study the Characterization of the Pulsed Laser Source with MMF	44
3.3	Experimental results of NMZI for chemical liquids	45
3.4	Experimental results of NMZI for biological liquids	48
3.5	Conclusions	51
3.6	Future works	52
	References	54
	Appendix A	A1
	Appendix B	B1
	Appendix C	C1
	Appendix D	D1
	Appendix E	E1
	Appendix F	F1
	Appendix G	G1



<b>List of Abbreviations</b>	
OFSN	Optical fiber sensor
WDM	Wavelength division multiplexing
FDM	Frequency division multiplexing
CDM	Code division multiplexing
OFI	Optical fiber Interference
FPI	Fabry- Perot interferometer
EFPI	Extrinsic Fabry Perot Interferometer
IFPI	Intrinsic Fabry Perot Interferometer
Sis	Sagnac interferometers
MI	Michelson interferometers
MZI	Mach-Zehnder interferometers
NMZI	Nested Mach Zehnder Interferometer
MFDs	Mode fiber diameters
LMA	Large Mode Area
MMF	Multimode fiber
DC	Double clad
SMF	Single mode fiber
PBG	Photonic band gap
PMD	Polarization Mode Dispersion
SPM	Self-Phase Modulation
XPM	Cross-Phase modulation
OKE	Optical Kerr Effect
RI	Refractive index
OSA	Optical spectrum analyzer
FWHM	Full Width Half Maximum.

<b>List of Symbols</b>		
<b>Symbols</b>	<b>Meaning</b>	<b>units</b>
A	Attenuation coefficient.	$\text{cm}^{-1}$
$\lambda_c$	central wavelength.	nm
$\Delta L$	The change in optical path length.	m
$\Delta\varphi$	Phase difference between the sensing arm and reference arm	-
$K_o$	Wave number	
$\Delta\phi_o$	Non -linear phase shift	
A	The cross sectional area.	$\text{m}^2$
C	speed of light in vacuum.	m/s
D	Diameter	$\mu\text{m}$
$L_{\text{eff}}$	The original length.	m
$n_{\text{eff}}$	effective refractive index.	-
$n_{co}$	Refractive index of core.	-
$n_{cl}$	Refractive index of cladding.	-
$I_r$	The intensity of reference arm	
$I_s$	The intensity of sensing arm	W
$P_o$	Output power.	W
PTX	transmitter power.	dBm
PRX	receiver power.	dBm
R	Radius.	$\mu\text{m}$
RI	Refractive index	
$\beta', \beta''$	Inverse group velocity dispersion	

<b>List of Tables</b>		
<b>Table No.</b>	<b>Table Name</b>	<b>Page No.</b>
Table (2.1)	Parameters for Pulse laser source	32
Table (2.2)	The optical specifications of MMF	34
Table (2.3)	Ethanol properties	38
Table (2.4)	Optical properties of Acetone	39
Table (3.1)	Opt wave results of etched MMF-MZI	43
Table (3.2)	Opt wave result of nested etched MMF-MZI	44
Table (3.3)	Opt wave result of Double cladd –MMF-NMZI	45
Table (3.4)	Experimental results of etched MMF-MZI at	45

	using chemical liquids	
Table (3.5)	Expermental results of NMZI using chemical liquids	46
Table (3.6)	Refractive indices of pregnant urine samples	47
Table (3.7)	Experimental results of etched MMF-NMZI at using sample pregnancy	49
Table (3.8)	Results of NMZI parameters	51

<b>List of Figures</b>		
<b>Figure No.</b>	<b>Figure Name</b>	<b>Page No.</b>
Fig (1.1)	schematic of multimode fiber ,(a) –step index,(b)-graded index	3
Figure (1.2)	a) Extrinsic FPI sensor made by forming an external air cavity, b) intrinsic FPI sensor formed by two reflecting components, R1 and R2, along fiber	6
Figure (1.3)	a) Basic configuration of a Michelson interferometer and ,b) Schematic of a compact in line Michelson interferometer	6
Figure(1.4)	a)A schematic diagram of Sagnac fiber interferometer ,b) in line MMF as Sagnac interferometer	7
Fig. (1.5)	a)A schematic configuration of MZI ,b) in line MMF as MZI [45]	9
Fig (1.6)	A schematic of $N$ -path MZI	10
Fig (1.7)	a) NMZI with 2arm ,b )NMZI with for arm	10
Figure (1.8)	The block diagram express the reasons of degradation of optical signal	12
Figure (1.9)	The block diagram of the attenuation losses.	14
Figure (1.10)	a)Waveguide dispersion , b)Material dispersion	15

Figure (1.11)	a) Intermodal dispersion in MMF step index, b) Intermodal dispersion in MMF graded index	15
Figure (1.12)	Variation in polarization states of an optical pulse as it passes through a fiber	16
Figure (1.13)	The effect of SPM on un-chirped pulse	18
Figure(2.1)	Scenarios of the work's steps	26
Figure (2.2)	Etched MMF using optgrating	27
Figure(2.3)	a) Simulation setup of DC-MMF MZI ,b)EDFA properties ,c)Opt grating properties	28
Figure(2.4)	simulation setup of NMZI	29
Figure (2.5)	a) The schematic diagram of the NMZI , -b)The photograph image of experimental setup for NMZI for detection system	30
Figure(2.6)	Schematic of Optical Coupler	32
Figure (2.7)	Front view for the MMF fiber under microscope	33
Figure (2.8)	Etching process experiment set up	34
Figure (2.9)	MMF under microscope after etching	35
Figure(2.10)	Optical spectrum analyzer FBGA regulator	36
Figure (2.11)	Optical Spectrum of Water	37
Figure (2.12)	Absorption spectrum of ethanol	38
Figure (2.13)	Absorption spectrum of acetone	39
Figure (2.14)	Digital refract meter	39
Figure (3.1)	Simulation results to design MMF etching segment , a) for 5min ,b) for 10min ,c) for 20min	42
Figure (3.2)	Opt wave output spectrum of DC –MMF MZI visualized with FBGA	43
Figure (3.3)	Pulsed laser source spectrum visualized with FBGA	44
Figure (3.4)	Etched MMF compare with pulse laser source	45

Figure(3. 5)	spectrum visualized with FBGA Output spectrum of NMZI for three different fiber diameter ,a) for distilled water, b)for ethanol ,c) for acetone	48
Figure(3.6)	Relationship between NMZI wavelength and three different refractive indices of liquids	48
Figure(3.7)	peak power spectrum of three pregnant with compared with non-pregnant at fiber, a) at fiberdiameter118.69 $\mu\text{m}$ ,b) at fiber diameter112.3927 $\mu\text{m}$ ,c) at fiber diameter72.532 $\mu\text{m}$	50
Figure(3.8)	The peak power of nested DC-MMF NMZI (urine pregnancy1,2,3 samples)compared with nested non-pregnant	51

***CHAPTER ONE***  
***Introduction and basic concepts***

# ***CHAPTER ONE***

## ***Introduction and Basic Concept***

### **1.1 General Introduction and Motivation**

Optical fiber sensor networks (OFSNs) are a strong tool for improved communications approaches sensing, and they can monitor temperature, strain, and other physical characteristics in a distributed or quasi-distributed manner [1]. The multiplexing technology of the optical fiber sensor is very simple to implement, which can lower the cost of a single point sensor, dramatically enhance the cost performance of the sensing system, and give optical fiber sensors more advantages than traditional sensors [2].

Multiplexing technology in communication employs the same interrogation system to query the measurement information of many sensors, considerably simplifying the system's complexity while also ensuring measurement accuracy and reliability. Time division multiplexing (TDM), frequency division multiplexing (FDM), wavelength division multiplexing (WDM), code division multiplexing (CDM), and space division multiplexing (SDM) are the most widely used multiplexing technologies [3-6]. Due to the short coherence length of laser interference, numerous sensors do not interfere with each other in their respective fields.

First, it provides considerable advantages in the multiplexing of fiber sensors capable of measuring absolute length and time delay [7,8]. Second, the short coherence length of the sensor signal reduces time-varying interference from stray light in the system [9]. Finally, many sensory signals can be coherently multiplexed into one signal without the need of complicated time division multiplexing or frequency division multiplexing algorithms [10, 11]. The sensor has an ability to measure different parameters such as pressure, force, strain, temperature, and others, as well as, has high sensitive immunity into electromagnetic interference and a simple structure. All advantages are used for different arrangements of in-line fiber interferometers in communications, optical modulation, pulse compression, and sensing applications. [12-15]. A typical conventional fiber Mach-Zehnder interferometer MZI consists of two fiber arms which are split and recombined by two optical

couplers. The conventional fiber Mach Zehnder interferometers have been widely employed as optical filters, fiber modulators, environmental sensors[7-9]. However, these two arms of MZIs have their own limitations, such as complicated structure, big size and high cost. To overcome the previous drawbacks, an in-line fiber MZI based on core-cladding-mode coupling has been proposed. Two light arms are both inside the same fiber in terms of core mode and cladding modes [16]. The cladding modes which have energy distributed in both core and cladding regions are excited by particular light steering elements, i.e. taper, core-offset, mode-mismatch, etc. Using only one piece of fiber, the in-line structure provides several advantages over conventional one such as compactness, high integrity, light weight, low cost and high stability [17]. It is feasible to determine the cladding refractive index variation with great precision by knowing how the two propagating modes will react to the cladding change and monitoring how much the phase difference between the two modes has changed. If the sensing waveguide is bio functionalized, this interferometer could be employed as a bio sensing device[18].Nested MZI configuration phase shifters are stacked in parallel along a line, which appropriate for hybrid construction is a revolutionary approach for implementing (OFSNs) [19]. nested has been designed using multi optical couplers for many applications such as switch based on balanced nested MZI .In communication, rapid detection is one of the most important requirements in the design of detection devices in all fields ,so in previous design not reusable for different rapid detection applications [20,21].This work introduced an In-line Nested Mach-Zehnder Interferometer using double clad with three different cladding thickness of multimode mode fiber fabricated using etching method .A double clad was implemented using three different refractive indices of chemical and biological liquid materials on the etched section area of the MM fiber to change the interference cavity refractive index.

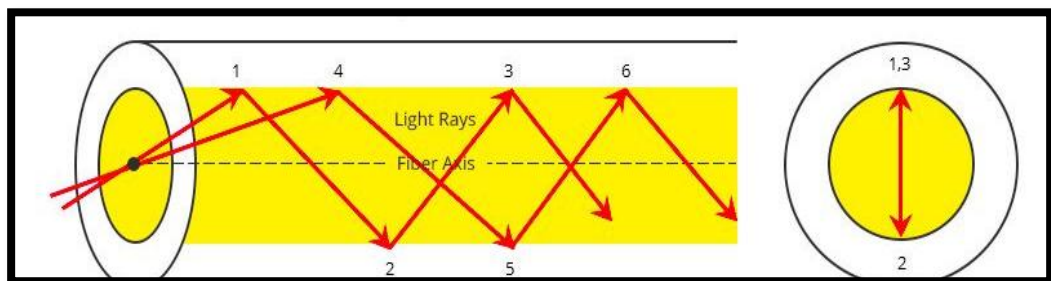
## **1.2 Aim of the work**

Design a rapid reusable detection system using etched multimode Mach Zehnder fiber interferometer as in line nested configurations.

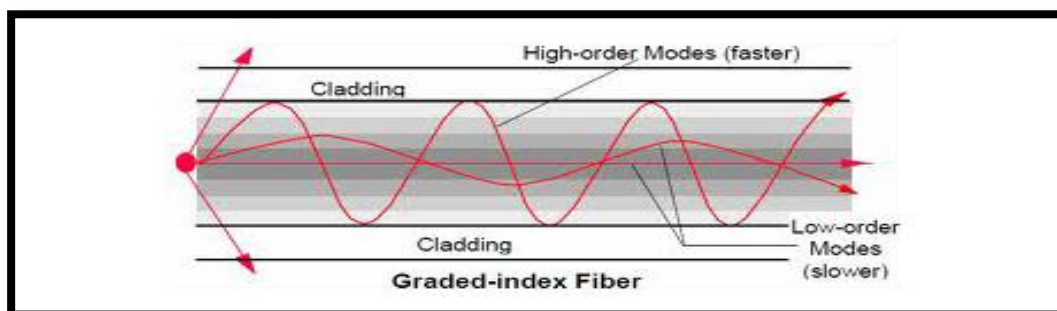


### 1.3 Multimode Fiber (MMF)

Multimode Fiber (MMF) is a particular type of fiber that is typically utilized in short-distance communication and has major core diameters and numerical aperture to given functional coupling process to light emitting diode LEDs " incoherent light sources like". Depending on the materials used and the manner of manufacture, the performance characteristics of this fiber type can vary significantly. These fibers are best suited for short-haul, low-cost applications with limited bandwidth. The attenuation of MMF fiber at wavelength of 850 nm, 40 dB /km ,while roughly losses 0.4 dB /km at a wavelength of 1310 nm. Two types of multimode fiber are multimode step index fibers and multimode graded index as shown in fig(1.1-a,b) [22] . Multimode fiber offers a broad range of purposes outside of the communications industry. Fiber-based sensors are used in medicine to aid in disease diagnosis, and they are also used in industry to monitor fluid movement and determine the distribution of temperature. fiber bundles are used as laser delivery systems, illumination light sources, and endoscopes, which have a long history in medical applications and are also used for remote viewing in dangerous areas such as nuclear reactors and network systems [23].



(a)



(b)

Fig (1.1) schematic of multimode fiber ,(a) –step index,(b)-graded index [24]

## **1.4 In Line Fiber Interferometers**

Interferometers operate according to the principle of scraping incidence of light [13]. Typically, an interferometer's to generate an interference pattern, a light beam is separated into two or more halves and then recombined. The constructive spots in the interference pattern correspond to the optical path difference between the two paths is an integer value of half wavelengths, while the destructive points correspond to the odd number of half wavelengths. If the difference in optical routes is an odd number of half wavelengths ,constructive and destructive interference[25]. There exist representative four types of fiber optic interferometers, called Fabry-Perot, Sagnac, Michelson, and Mach-Zehnder. For each type of interferometer, the operating principles and the fabrication processes are presented.

### **1.4.1 In Line Fabry-Perot Interferometer**

In general, a Fabry-Perot interferometer (FPI) comprise of two parallel reflecting surfaces separated by a certain distance [26]. Interference occurs due to the multiple superpositions of both reflected and transmitted beams at two parallel surfaces [27,28]. It's also known as an etalon. Extrinsic and intrinsic Fabry-Perot interferometers are the two types of Fabry-Perot interferometers.

- 1- The intrinsic Fabry-Perot interferometer (IFPI) fiber sensors have reflecting components within the fiber itself. [29].The extrinsic structure is excellent for obtaining a high fineness interference signal since it can use high reflecting mirrors. Furthermore, the fabrication is straightforward and does not necessitate the use of expensive machinery. EFPI has the drawbacks of careful alignment, limited conjugation functionality , and packing issues[30].
- 2- Reflective components are built into the intrinsic Fabry-Perot interferometer (IFPI) fiber sensors. For example, inherent FP interference can occur when reflectors are generated within a fiber by various methods. Manufacturing, fiber Bragg gratings (FBGs), chemical etching, and thin film deposition are all examples of thin film deposition techniques. can all be used to create the intrinsic FPI's local cavity [30], as shown in Fig (1.2)The existence of the MMF as an FPI at a

given length can collimate the divergent light beam and compensate the light loss inside the FP cavity.

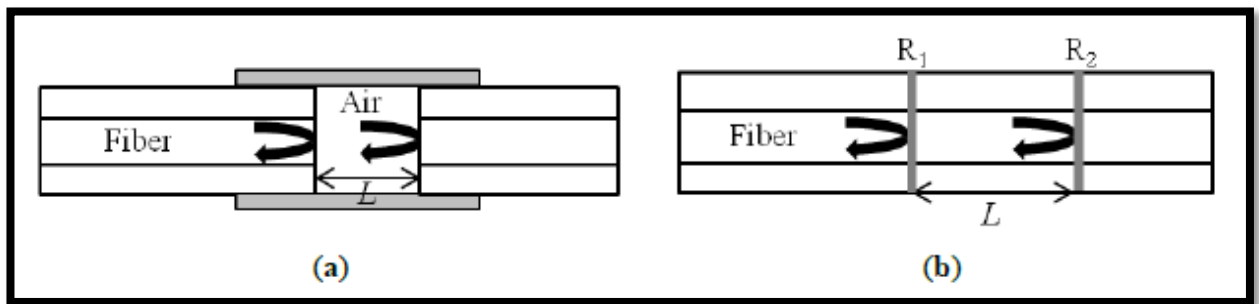


Fig (1.2) Fabry Perot interferometer a) Extrinsic FPI, b) intrinsic FPI sensor created by,  $R_1, R_2$  [30]

### 1.4.2 In Line Michelson Interferometer

A schematic of conventional Michelson Optical Fiber Interferometer (OFI) is depicted in Figure (1.3-a,b), a part of the core mode beam is coupled to the cladding mode(s), which is reflected along with the uncoupled core mode beam by the common reflector at the end of the fiber [25].

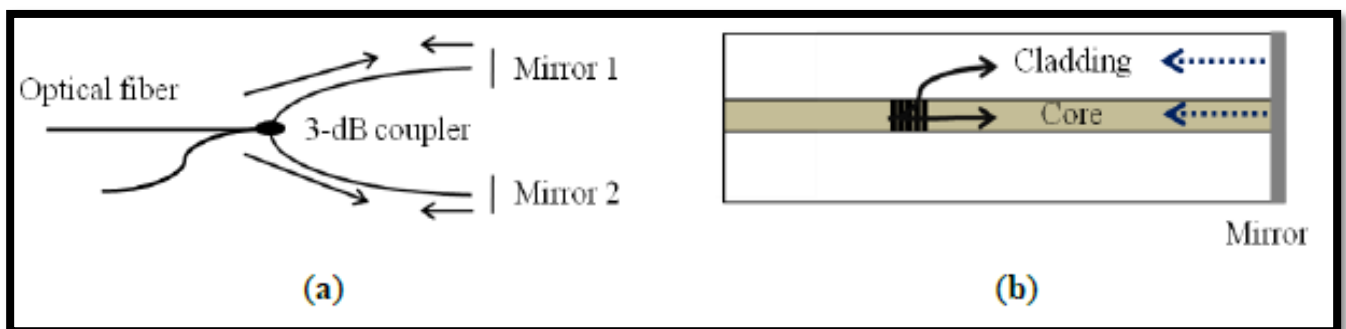
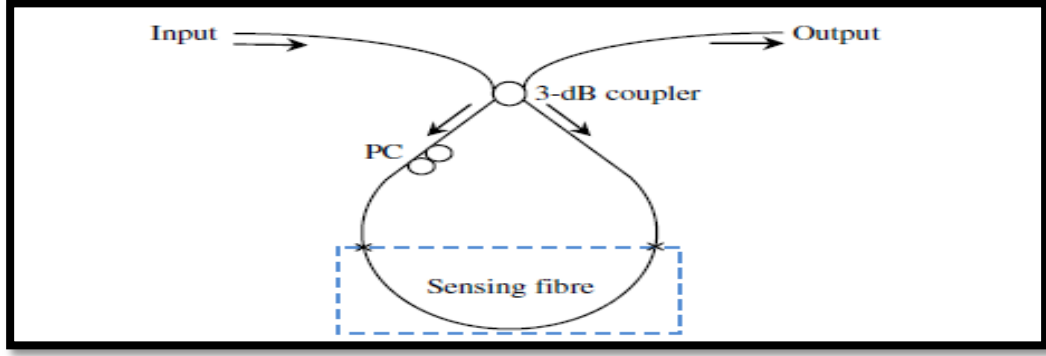


Figure (1.3) In line Michelson interferometer ,a) A compact in-line Michelsonn interferometer ,b Basic setup of Michelson interferometer [25].

### 1.4.3 In Line Sagnac Interferometer

Sagnac interferometer consists of an optical fiber loop, along which two beams are propagating in counter directions with different polarization states. As schematically illustrated in Figure (1.4), the input light is split into two directions by a 3 dB fiber coupler two counter-propagating beams are combined again at the same coupler. Unlike other fiber optic interferometers, the Optical path difference OPD is determined by the polarization dependent propagating speed of the mode guided along the loop. To maximize the polarization-dependent feature of SIs, birefringent fibers are typically utilized in sensing parts.



**Figure(1.4) Schematic of a Sagnac fiber interferometer [32]**

A polarized control system (PC) attached to the beginning of the sensor fiber adjusts the polarizations. The signal at the fiber coupler's output port is determined by interference between beams polarized along the slow and fast axes. The interference phase is simply expressed as [32].

$$\delta_{SI} = \frac{2\pi}{\lambda} BL \quad , \quad B = |n_f - n_s| \quad (1.1)$$

Where  $B$  is the Birefringent coefficient of the sensing fiber,  $L$  is the length of the sensing fiber, and  $n_f$  and  $n_s$  are the effective indices of the fast and slow modes, respectively. The clockwise (CW) and counterclockwise (CCW) modes are in phase with one another in a non-spinning Sagnac interferometer, but the optical paths of one of the modes are shortened and the other is lengthened in a rotating Sagnac arrangement due to the rotating velocity. The Doppler frequency difference between the CW and CCW modes can be used to perform analysis. The beating frequency of The detector output frequency can be switched between CW and CCW modes. When the rotating axis is aligned with the optical fiber coil axis, the phase difference of CW is decreased and CCW modes is:

$$\Delta\theta = 8\pi NA\omega/\lambda c \quad (1.2)$$

where  $\lambda c$  is the central wavelength ,  $A$  is the sectional area of interferometer ,  $N$  is the fiber trip number ,  $\omega$  is the angular velocity .

#### **1.4.4 In Line Mach-Zehnder Interferometers (MZI)**

Mach-Zehnder interferometers have been utilized in a wide range of sensor purposes due to their versatility. Incident light is separated into two arms by a fiber coupler, which are

then recombined by another fiber coupler [33]. The sequenced light has an obstruction element according to the path length distinction between the two arms. (1.5-a). In line MZIs, there are many different sorts of designs that use the same types of fibers, such as PCF, SMF, MMF, NCF, etc.

The collapsed region in the current MMF between two single mode fibers causes the input light to split into the MMF's core and cladding, resulting in light propagating as core and cladding modes, respectively. and obtained high sensitivity that described by equation(1.3) with generated phase shift,  $\Delta\varphi$ , between the two interferometer's arms [33].

$$I = I_r + I_s + 2\sqrt{I_r I_s} \cos(\Delta\varphi) \quad (1.3)$$

Where  $I_r$  and  $I_s$  are the intensities of reference and sensing arm. The different in phase between the sensing arm and reference arm is described by :

$$\Delta\varphi = \frac{2\pi\Delta L n_{\text{eff}}}{\lambda c} \quad (1.4)$$

Where  $\Delta L$  is the change in optical path length ,  $n_{\text{eff}}$  is the "effective refractive index" of the mode and it will be given as

$$\Delta n_{\text{eff}} = n_{1\text{eff core}} - n_{2\text{eff cladd}} \quad (1.5)$$

Figure (1.5-b) shows a schematic diagrams of the in-line fiber MMF MZI ,the first collapsed region acts as a beam splitter coupler where the core and cladding modes are excited in MMF simultaneously while the second collapsed region acts as combiner coupler. The core mode and cladding modes travel along the MMF length (L) with different speeds. Since these modes are characterized by their effective refractive indices ( $n_{\text{core}}$  and  $n_{\text{clad}}$ ) therefore, a relative group delay is developed after the propagation therefore the number of modes because of the usage of different refractive indices, it is necessary to obtain the number of excitation of higher modes according to the following equation in the sensing area of the design [ 34].

$$M = V^2 / 2 \quad (1.6)$$

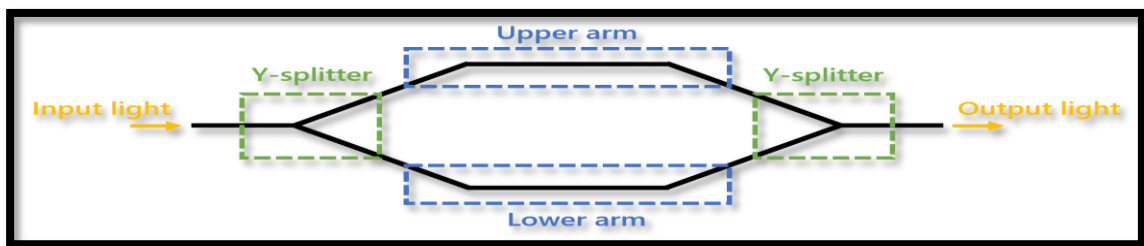
where V is normalysed frequency which calculated from following equation

$$V = 2 \frac{\pi a}{\lambda c} \sqrt{n_1 - n_{\text{eff}}} \quad (1.7)$$

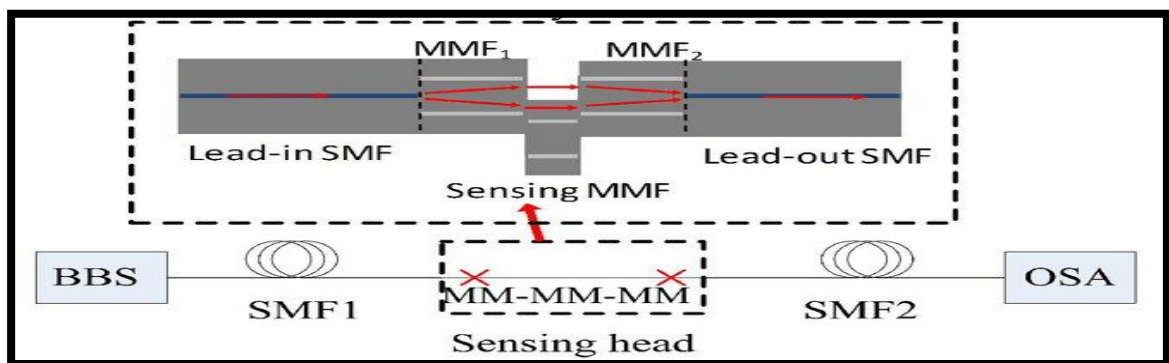
Where  $a$  is core radius,  $n_1$  is core refractive index and  $n_{eff}$  is an effective of cladding refractive index,  $\lambda_c$  is central wavelength in (nm)

A well-known idea in communication is that a narrower pulse in the time domain has a wider spectrum in the spatial domain. As a result, the compression factor (CF), which is the ratio of the input signal full width at half maximum to the output signal full width at half maximum [12].

$$CF = \frac{FWHM_{i/p}}{FWHM_{o/p}} = \frac{\Delta\lambda_{FWHM-i/p}}{\Delta\lambda_{FWHM-o/p}} \quad (1.8)$$



(a)



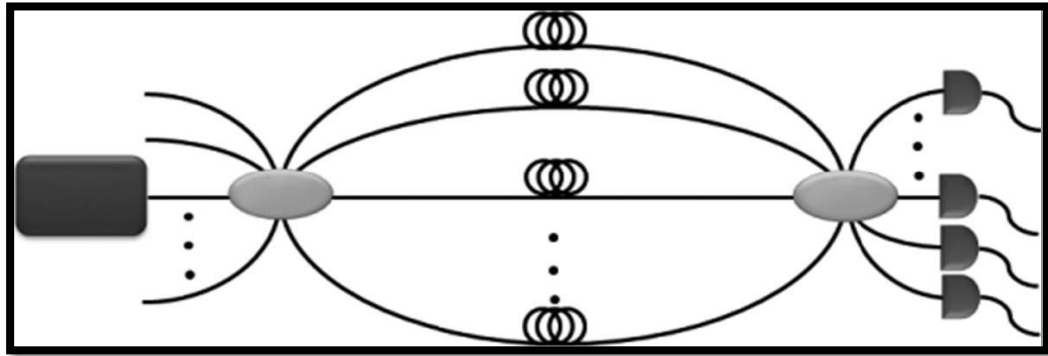
(b)

Fig. (1.5) a) A schematic configuration of MZI, b) in line MMF as MZI [33]

## 1.5 The operation principles of Nested Mach-Zehnder Interferometer

In communication systems high-speed switching, the phase shifter of a MZI switch is typically designed to higher interconnect bandwidth. The rapid growth of data increased pressure on data center therefore it require larger switching capacity, data switching technologies develop high-performance optical switching technologies for data center communication applications. In MZI the optical power in the two interferometer arms of the switch is unbalanced, leading to a large crosstalk at the cross output port [35]. In

order to suppress crosstalk, the optical power inside a MZI switch needs to be balanced. Recently, a solution using a nested MZI structure with a variable optical attenuator was proposed [36]. presented a Nested Mach- Zehnder interferometer (MZI), which was built by putting a smaller MZI in the upper arm of a larger MZI [37] as shown in Fig (1.6).



**Fig (1.6) A schematic of  $N$ -path MZI**

The structure of Nested Mach-Zehnder interferometer (NMZI) is including  $N \times N$  optical coupler, operating an input and output shown in Fig (1.7)

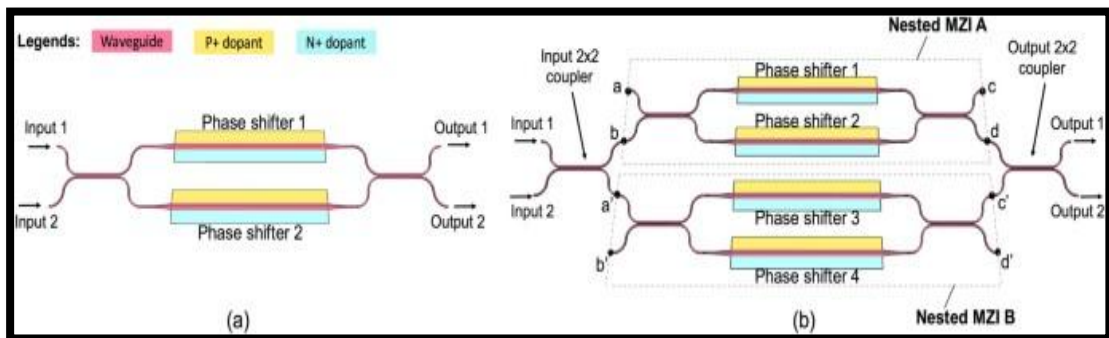


**Fig (1.7) Nested MZI ,a) Two arm nested ,b) Four arm nested [38]**

Because of modes in core were a greater refractive index than modes in cladding [39], the interference modality which is dependent on the extent of the optical path, indicates the displacement between two arms of the interferometer in fig(1.6) a phase tuner will apply an outline  $\Delta\phi$ , i.e., 1, 2, or 3, to the photon via one of the three paths (PT) we can control whether the three channels' influence is productive or detrimental by adjusting these three external phases [37]. In the absence of polarization altering devices, the coupler can be described

by a  $N \times N$  matrix for linear polarized (LP) fields.. According to eq (1.9) the amount of intensity of  $N \times N$  is given as

$$I_n = \frac{I_0}{n} \llbracket 3 + 2 \cos(\varphi_{12} + \theta_n) + 2 \cos(\varphi_{23} + \theta_n) + 2 \cos(\varphi_{31} + \theta_n) \rrbracket$$

$$n=1,2,3 \quad (1.9)$$

where  $(\theta_1, \theta_2, \theta_3) = (0, -2\pi/3, 2\pi/3)$ . In the presence of loss or gain in optical fibers, the optical path matrix is  $P$  where  $n = 1, 2, 3$  is the transmission coefficient of the  $n$ th optical fiber branch. Since the slopes and main peaks are steeper in an  $N$ -path interferometer, it's sensitivity is higher than a conventional MZI. In addition, the phase differences  $\varphi_{ij}$  being sensitive to the environmental parameters such as temperature and strain. Also the higher cladding sensitive modes are change in the rounding environment. In MMF different modes of multimode fibers have different velocities and the modal interferometers are established on the basis of this effect (dispersion). Typically,  $LP_{01}$  and  $LP_{11}$  modes or  $HE_{11}$  and  $HE_{21}$  modes of step index optical fibers can be employed to design the modal interferometers From the wave equation[40]. :

$$E_x = E_0 \exp^{j(\omega t - kx)} \quad (1.10)$$

where the  $k$  is wave number is known as

$$k = \omega/v = 2\pi/\lambda c, \quad (1.11)$$

### 1.5.1 Nested Mach Zehnder Interferometer based on Double Clad Multimode Fiber

The techniques of double clad are purely based on the excitation to higher order modes of fibers. They are applied to pulses that are initially chirped, bandwidth not limited. The invention of double-clad (DC) active optical fiber initiated the rapid development of high-power fiber laser systems ,also new approach for the suppression of undesirable modes in DC optical fibers with an increased core-to-cladding diameter ratio.

Most method is based on the introduction of high-index absorbing inclusions into the first fiber cladding. Properly adjusted inclusion parameters disturbed the undesirable modes shape and increased their propagation losses due to absorption of the power



located inside the inclusions . The most recent in the development of large-mode-area (LMA) fiber allowed further scaling of the peak power to the MW level directly after optical fiber amplifiers and to the GW level after compression of nanosecond to femtosecond pulses durations [41] . Linear and non –linear properties of different refractive indices of liquids have been achieved to etched MMF to improve DC fiber have been proposed .

### 1.6 The Degradation of Signals in Optical Fiber

The main reason for degradation of optical signals after propagated are described in the block diagram which is shown in figure(1.8)

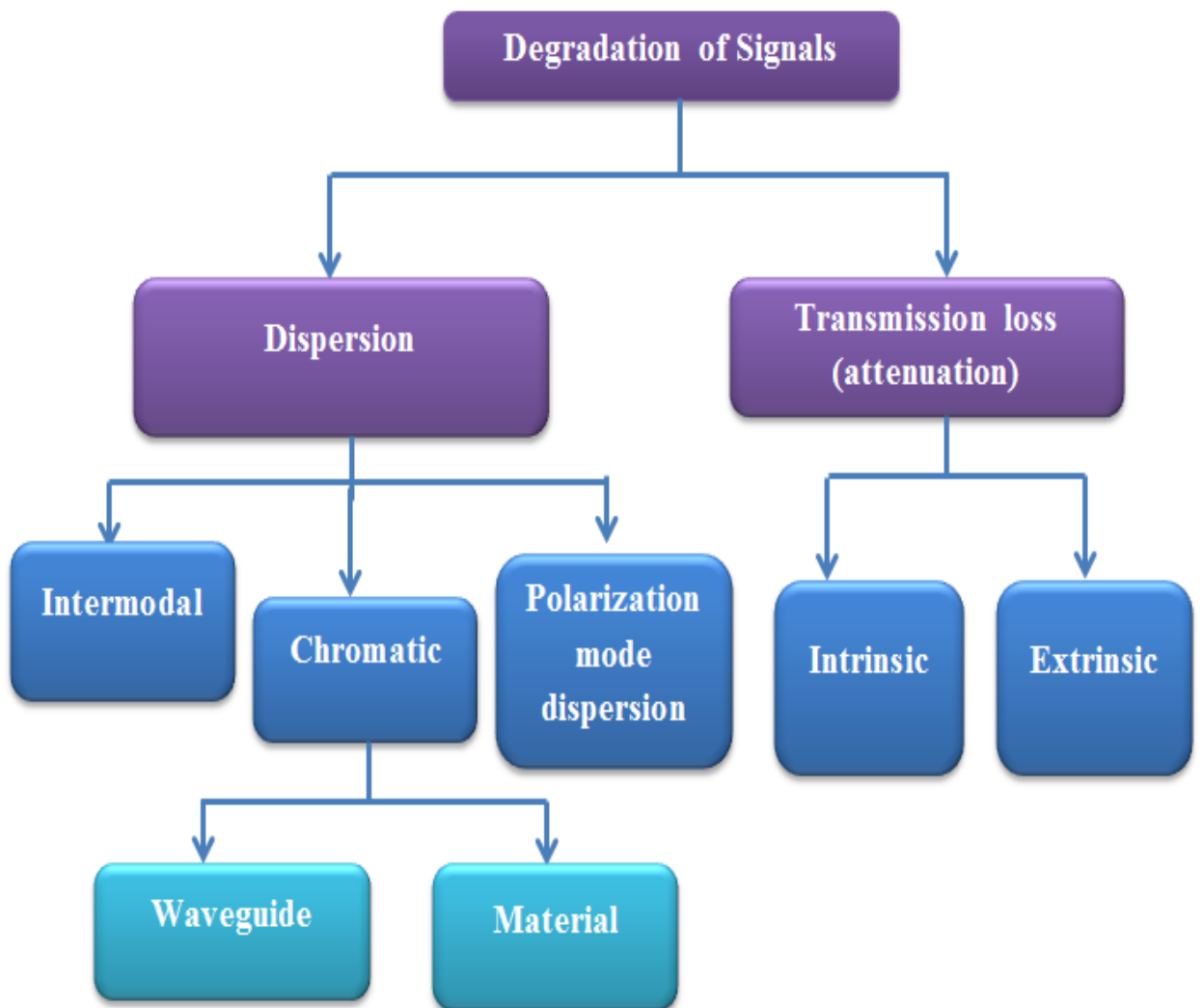


Figure (1.8) The reasons of degradation of optical signal[42]

### 1.6.1 Transmission loss (attenuation)

The losses of optical signals transferred over the optical fiber are the most important factors in optical communication system. The minimal loss for fused silica, whose wavelength is around 1550 nm, is slightly less than 0.2 dB/km[43,44]. These losses were classified into intrinsic and extrinsic losses as shown in Figure(1.9)

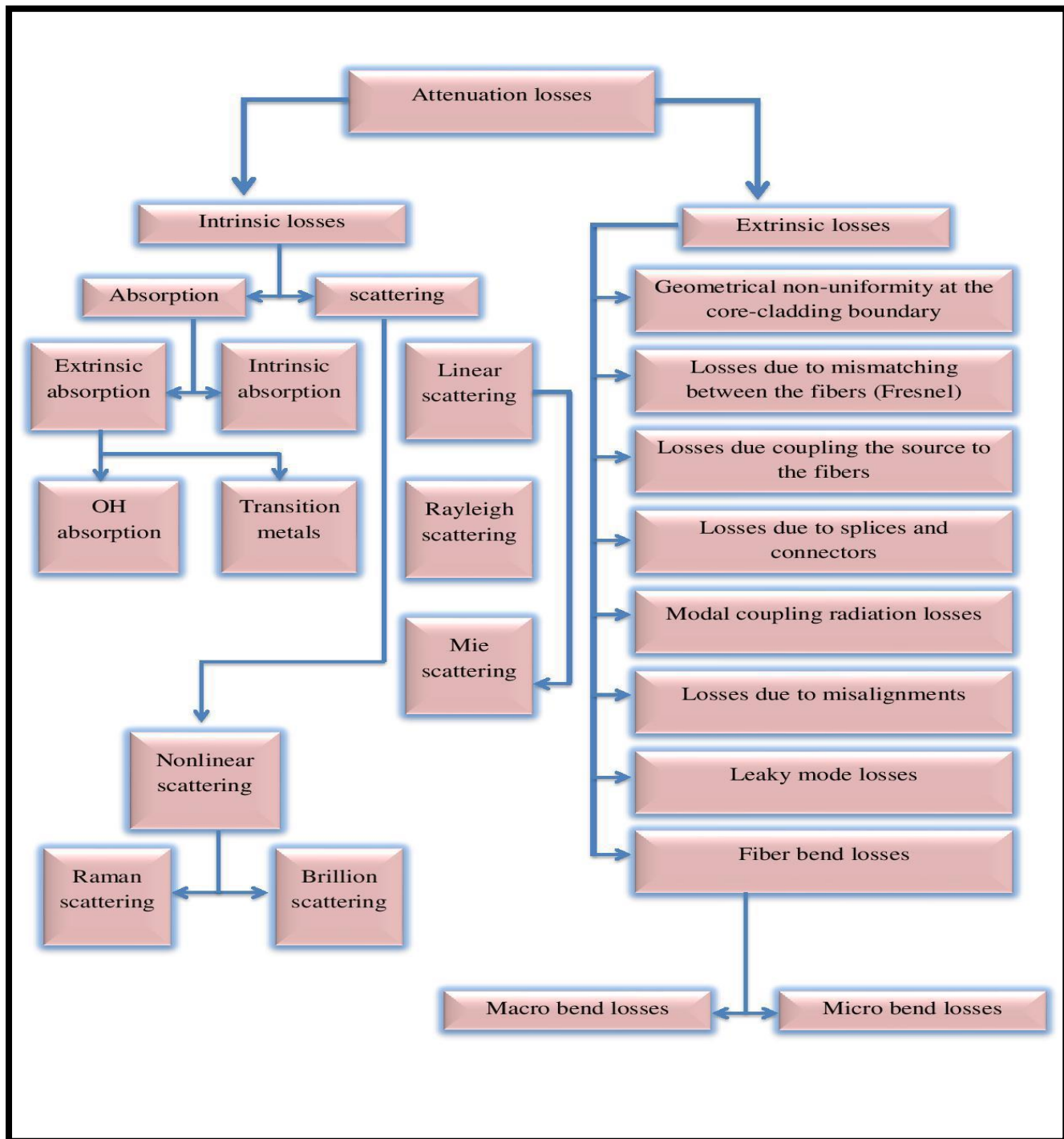


Figure (1.9) The attenuation losses[42,43].

Figure (1.9) of the Attenuation is divided into two kinds: Intrinsic and Extrinsic losses, as which are presented in equ (1.12), so that the attenuation or the loss ( $\alpha$ ) represent energy loss during the transmission of the data in the fiber and it can be defined as

$$\text{Loss } (\alpha) = -10 \log(P_o / P_i) \quad (1.12)$$

Where:

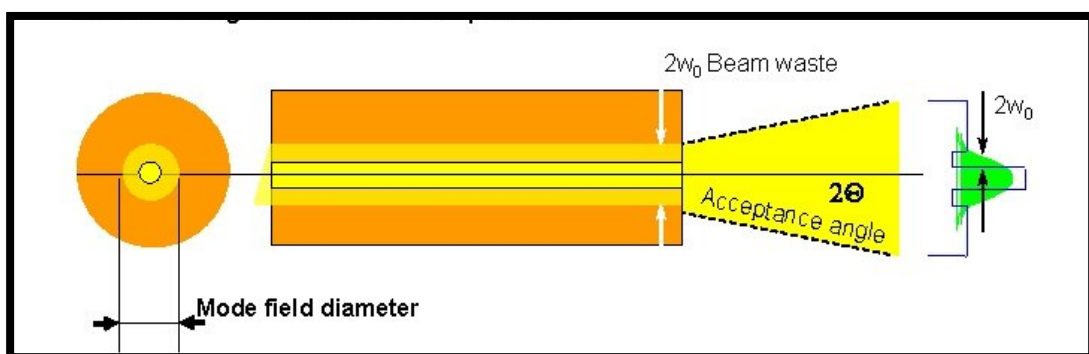
$P_i$  is the input power,  $P_o$  is the transmitted (output) power.

### 1.6.2 Dispersion

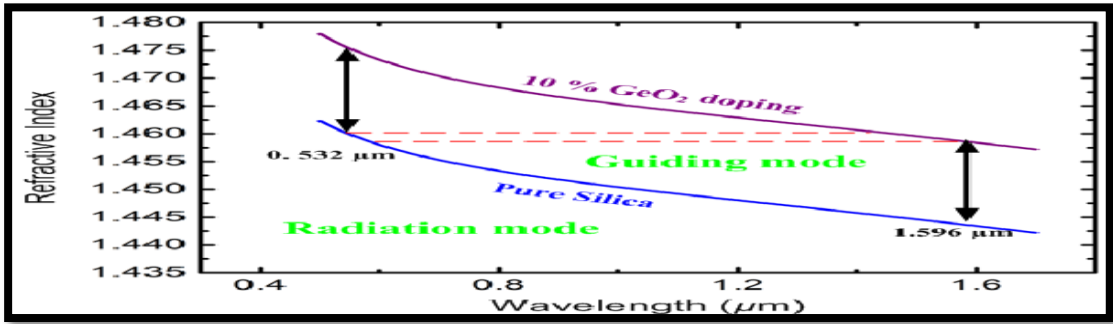
In the field of optical waveguides, dispersion is a general term referring to all phenomena causing these pulses to spread while propagating and they ultimately overlap, light pulses could not be distinguished by the receiver [44]. There are essentially three causes of dispersion.

#### 1.6.2.1 Chromatic Dispersion

Chromatic dispersion is an important phenomenon in the propagation of short pulses in optical fibers[45]. It is caused by delay differences among the group velocities of the different wavelengths composing the source spectrum[46]. The consequence of the chromatic dispersion a broadening in the transmission of the impulses . Chromatic dispersion is essentially due to two contributions, mat-erial dispersion and waveguide dispersion as shown in Fig (1.10-a,b)



(a)



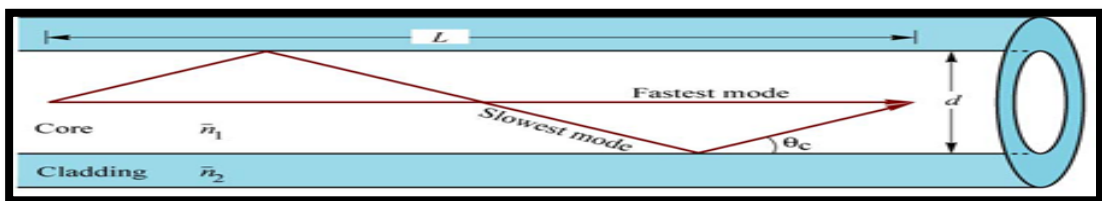
(b)

Figure (1.10) Dispersion spectrum a) Waveguide dispersion, b) Material dispersion [45]

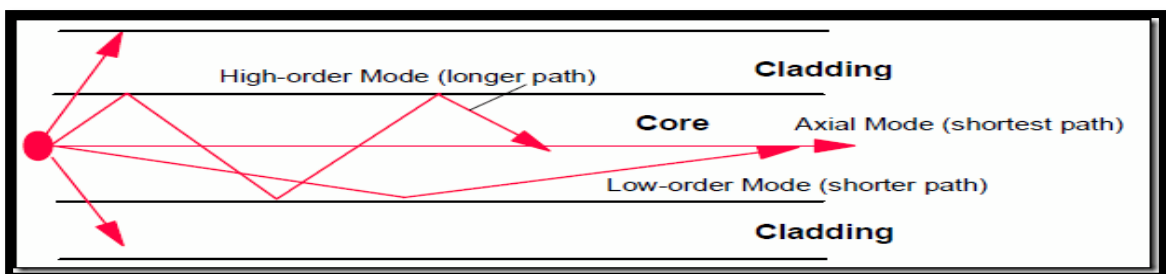
As presented in Figure (1.10-a,b) material dispersion ( $M_D$ ) occurs when the refractive index varies the optical frequency. The dispersive features of the waveguide cause waveguide dispersion ( $W_D$ ) [47].

### 1.6.2.2 Intermodal Dispersion

Intermodal dispersion is that type of dispersion that results from the varying modal path lengths in the fiber [45]. In multimode fiber the propagation delay differences between modes occurs because rays follow various paths through the fiber and consequently at different times reach the other end of the fiber [46] as shown in Fig (1.11-a,b).



(a)



(b)

Fig(1.11) Intermodal dispersion a) in MMF step index, b) in MMF graded index

In a step-index multimode fiber, the center ray with a  $0^\circ$  incident angle travels fastest straight down the fiber. The ray which is incident at the critical angle travels slowest. The time delay between these two modes is given by following equation :

$$\Delta\tau = L(n_1-n_2)/c[1-(\pi/V)] \quad (1.13)$$

where  $n_1$  is refractive index of the core,  $n_2$  is refractive index of the cladding,  $L$  is the length of the fiber,  $V$  is normalized frequency .

In graded-index profile multimode fiber, the modal dispersion calculation becomes a little more complicated since we have to account for the inhomogeneous velocity of the light in the fiber as well as the sinusoidal paths. Although the higher-order modes need to travel longer path lengths, their average velocity is also higher than the light ray at the center (graded-index fiber has highest refractive index at the center and then gradually decreases toward the cladding).When comparing the modal delays of step-index and graded-index fibers, the modal dispersion of graded-index fiber is less than that of step-index fiber. The fact that a graded-index multimode fiber has a graded index above a step-index multimode fiber of the same size is one of its main advantages [45].

### 1.6.2.3 Polarization Mode Dispersion

A fundamental property of an optical signal is its polarization state. Polarization refers to the electric-field orientation of a light signal, which can vary significantly along the length of a fiber, as illustrated in Figure (1.12).

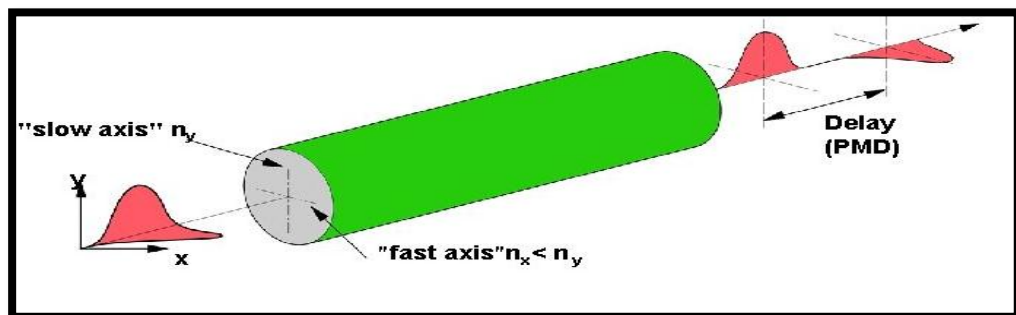


**Figure (1.12) Variation in polarization states of light pulse inside the fiber [46].**

A varying birefringence along its length will cause each polarization mode to travel at a slightly different velocity and the polarization orientation will rotate with distance. The resulting difference in propagation modes will result in pulse spreading that is called Polarization Mode Dispersion (PMD) [48,49].

### 1.6.3 Nonlinear phenomena

When a material is exposed to a powerful electromagnetic field, the material's response is nonlinearly dependent on the strength of the applied optical field. The polarization  $P$  generated by electric dipoles is not linearly proportional to the electric field  $E$ , but it fulfills the more general relation by writing  $P$  as a power series in  $E$  as in equation (1.14).

$$P = \epsilon_0 (\chi^{(1)} E + \chi^{(2)} EE + \chi^{(3)} EEE + \dots) \quad (1.14)$$

$\chi$  ( $\chi = 1, 2, \dots$ ) is the  $\chi^{\text{th}}$  order susceptibility and a tensor of rank  $\chi + 1$  of the medium, where  $\epsilon_0$  is the permittivity of free space. The linear susceptibility  $\chi^{(1)}$  is the most important factor in  $P$ . Nonlinear effects such as third-harmonic production, Four wave mixing FWM, two-photon absorption, and NL refractive index are all caused by the term  $E^3$  [50]. The only nonlinear component that is meaningful for us is  $E^3$  as the higher order terms in the power series become less and smaller. The varied impacts of the PCF, such as intensity dependent refractive index, self-phase modulation (SPM) effective length, and cross section area, will be briefly explained in the following subsections caused by  $\chi^{(3)}$ .

#### 1.6.3.1 Refractive Index Based on Intensity

Refractive Index Based on Intensity in the presence of this type of nonlinearity can be described as:

$$n(\omega, E^2) = n(\omega) + n_2(\omega) E^2 \quad (1.15)$$

where  $n(\omega)$  is the linear, weak-field refractive index and  $n_2(\omega)$  is the nonlinear refraction coefficient, and equation (1.15) is the linear, weak-field refractive index. To avoid confusion with the ordinary, weak field refractive index, a bar is placed over the refractive index  $n$ . By analogy with the electro-optic Kerr effect in which changes in the refractive index of a material are proportional to the square of the strength of an applied static field.

### 1.6.3.2 Self-Phase Modulation

SPM (self-phase modulation) is a NL Interactions of light and matter. When an ultra-short pulse of light travels through a medium, the optical Kerr condition caused the medium's refractive index to fluctuate. The pulse's phase shifts due to the change in refractive index, resulting in a shift in the pulse's spectrum. [51].

Many optical materials' refractive index  $n$  has a pedestrian relationship with light intensity  $I_{eff}$  (equivalent to optical power density in the fiber) provided by [50,51]:

$$n = n_0 + n_2 I_{eff} = n_0 + (n_2 p/A_{eff}) \quad (1.16)$$

where  $n_0$  is the material's ordinary refractive index and  $n_2$  is its non-linear refractive index. The factor ( $n_2$ ) for silica ranges from 2.2 to 3.4  $10^{-20} \text{ m}^2/\text{W}$ , while the factor ( $n_2$ ) for air is 241021  $\text{m}^2/\text{W}$  [52]. The intensity of a light domain modulates the phase of the optical domain, and the optical domain modifies its own phase [53]. The pulse's nonlinear phase shift is calculated using the equation NL:

$$\Phi_{NL} = (2\pi n_2 L_{eff} I)/\lambda \quad (1.17)$$

where  $L_{eff}$  is the fiber effective length. The total phase shift  $\phi$  experienced by the optical field. This phase shift varies with time for pulses and each optical pulse become chirped, which means a pulse propagates along the fiber, its spectrum changes because of SPM as shown in Fig (1.13)

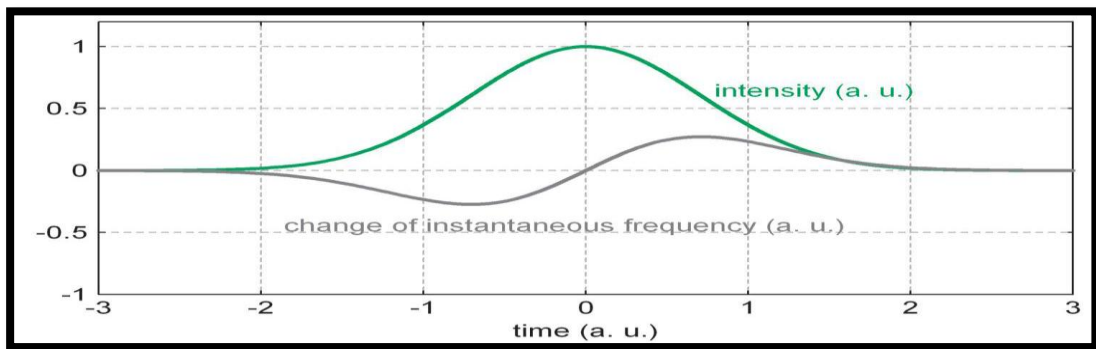


Fig (1.13 )The effect of SPM on un-chirped pulse [50].

### 1.6.3.3 Stimulated Raman Scattering

The nonlinear process of stimulated Raman scattering (SRS) can result in the formation of new spectral lines. The third-order susceptibility is responsible of SRS. It is caused

by a mechanism known as stimulated inelastic scattering, in which the optical field transmits some of its energy to the medium, resulting in the generation of a photon [51]. The Spontaneous Raman effect happens when a beam of light illuminates any molecular medium and the scattered light is spectroscopically investigated. The energy levels of the process) The Raman Effect scatters just a small fraction of the incident optical field into other fields. The new frequency components that have been transferred to lower frequencies are referred to as the Stokes lines and the anti-Stokes lines are those that have been moved to higher frequencies. The vibrational modes of molecules control the degree of frequency shift. [50].

#### **1.6.3.4 Effective length**

The nonlinear interaction is determined by the fiber's length of transmission and cross-sectional area. The higher interaction sharper and the longer link length are effect of nonlinearity. However, the fiber attenuation, signal's power drops it travels over the link. As a result, the majority of NL effect Early in the fiber span, effects appear and diminish away as the signal travels. A simple model that assumes the power is constant along a specified effective length can be used to characterize the impact of nonlinearities., as indicated by Leff. Suppose that  $P_0$  is the power delivered into the fiber, and that  $p(z) = p_0 \exp(-z)$  signifies the connection, and that is the fiber a attenuation[51].

#### **1.6.4 Nonlinearities phenomena in MMF –MZI**

We established the first physical case addressed by Manakov's equation generalized is propagation in a degenerate group of randomly correlated spatial modes of a multi-mode optical fiber. The equation's of nonlinear parameter was defined in terms of a generic optical fiber's standard parameters.

Mathematical form serves as a beginning step for research of NL effects in MMF transmission, both analytically and numerically. Its significance, as well as recent interest in spatially multiplexed transmission using multi-mode and multi-core optical fibers. As



a result, Manakov's equation was shown as following equation[54] :

$$\frac{\partial E}{\partial Z} = -\beta' \frac{\partial E}{\partial t} - i \frac{\beta''}{2} \frac{\partial^2 E}{\partial t^2} + i\gamma K |E|^2 E. \quad (1.18)$$

The terms  $\beta'$  and  $\beta''$  are the inverse group velocity and the dispersion coefficient,  $\gamma$  is usual non-linearity coefficient .

The physical process due to saturation of absorption near 980 nm. a phase shift occurs at the signal wavelength causing switching. With only a few mill watts of pump power, on the other hand, phase changes of or more can be created. The cross phase modulation XPM-induced phase shift should be differentiated from this mechanism Nonlinear.

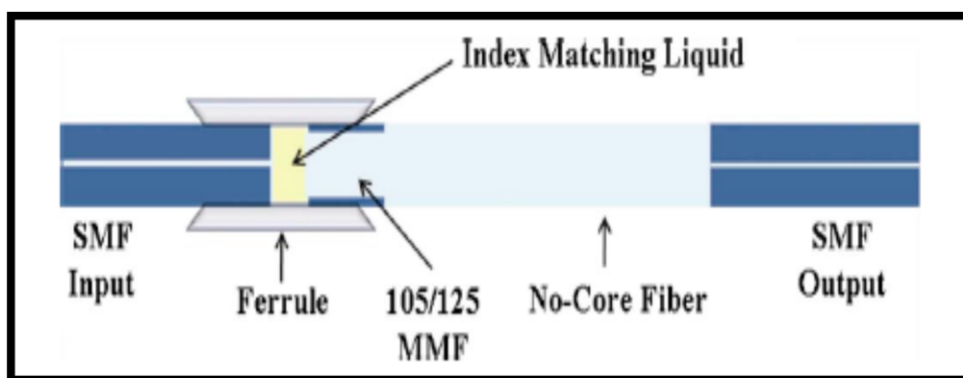
In nonlinear MZI applications, phase shifts caused by SPM or XPM are exploited. The biggest benefit is that many MZIs can be cascaded because the remaining channels appear at the MZI's output end (rather than being reflected).The disadvantage is that, in order to eliminate oscillations caused by environmental changes, active stabilization is frequently required [50,51].

## 1.8 Literature survey of Nested structure

In the following, a literature survey is given for some important research works in the field of all optical sensors using Multimode fiber as a sensor head that are most related to this work .

### 1- J. E. Anthony, Casal-Guzman, D. A. May, R. Silva's-Aguilar, and P. LiKamWa.2010) [52].

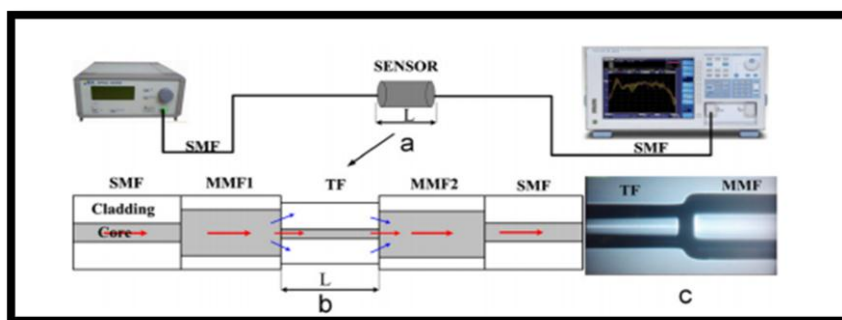
- **Fiber interferometer type** :Mach Zehnder interferometer
- **Technique used** : increase the length of the MMF, a cuvette filled with refractive-index-matching material is used.
- **Fiber type**: MMF
- **Experimental result** :Tuneability 30 nm
- **Experimental work**



Schematic of the tuning mechanism for the tunable MMI fiber filter.

### 2-Deming Liu (2012)[53]

- **Fiber interferometer type** : Mach Zehnder interferometer
  - **Technique used** : single mode MMF thinned SMTMS (multimode-thinned-multimode-single-mode) fiber
- **Experimental result** : Sensitivities of -16.1936 nm/RIU and 0.053 nm/Co and 23.0473 nm/RIU and 0.0575 nm/Co.



**3- Xiaoliang Wang , Daru Chen; Haitao Li; Gaofeng Feng; Junyong Yang  
(2017)[55]**

**Fiber interferometer type :** Mach-Zehnder Interferometer (MZI)

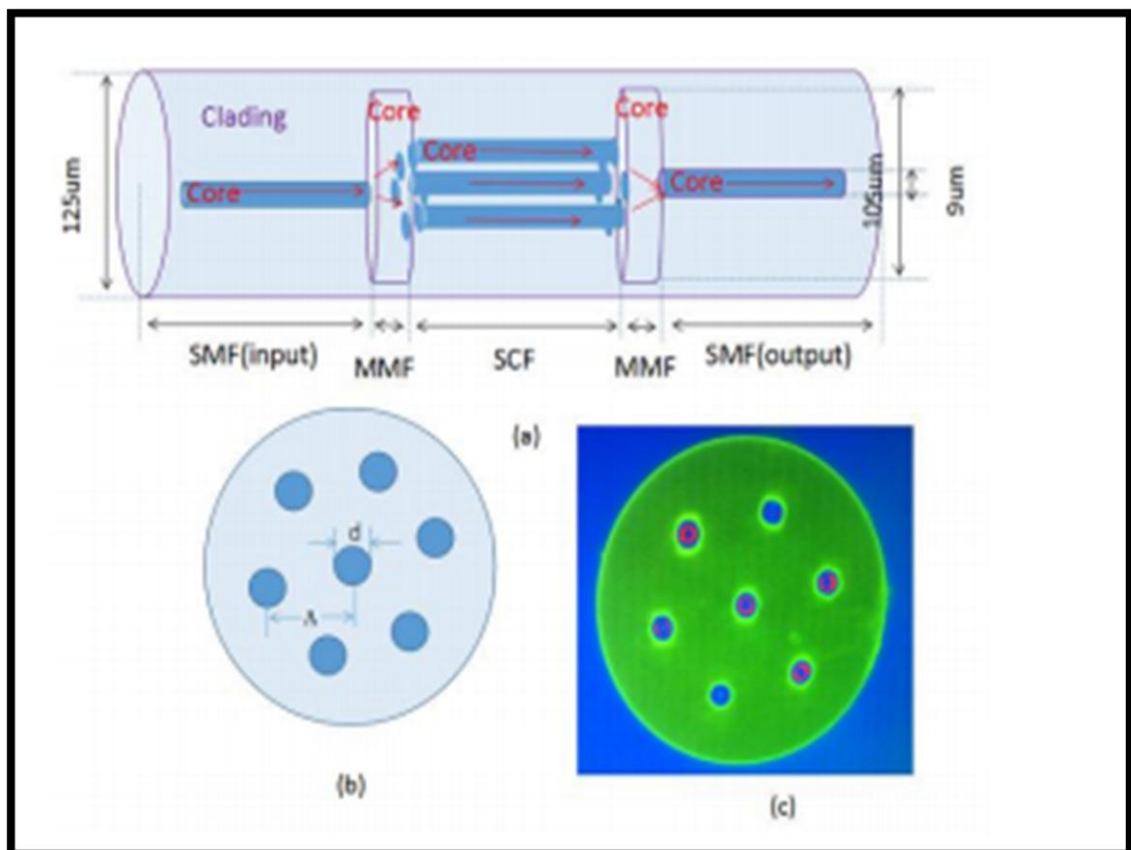
**Technique used:** an extremely sensitive glucose detection refract meter has been (.developed

**Fiber type :** seven-core fiber (SCF) and two segments (MMFs )

**Wavelength :**1550nm

**Experimental result:** The temperature and curvature sensitivities are 55.81 pm/°C and 31.54 nm/m<sup>-1</sup> , respectively.

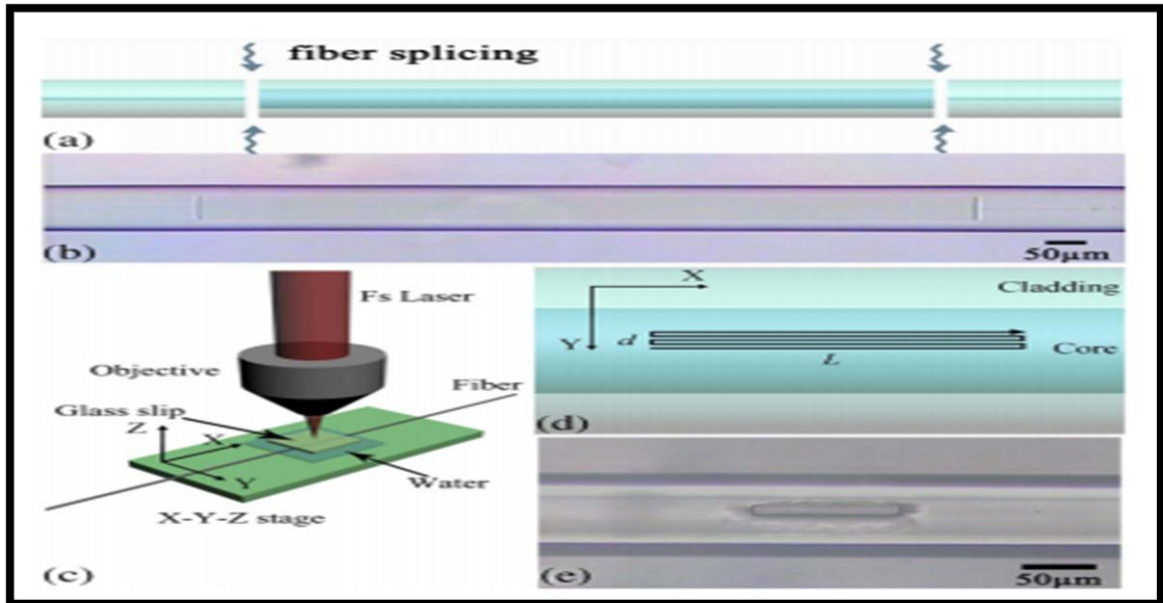
**-Experimental work**



**a)Schematic diagram of the proposed MZI based-on SCF. (b)A  
cross sectional view of SCF. (c) Micrograph of the SCF**

#### 4- yi liu, guoqiang wu, renxi gao, and shiliang qu.(2017)[56]

- **Fiber interferometer type :** Mach-Zehnder Interferometer (MZI)
- **-Technique used :** liquid RI sensing
- **-Fiber type :** single-multi-single mode fiber (SMSF)
- **-Wavelength :** femtosecond laser
- **-Experimental result:,** Ultrahigh sensitivity (9756.75 nm/RIU)
- **-Simulation work**



- a) A segment of the MMF was spliced in between two SMF sections. (b) The SMSF's splicing ) result. (c) Setup for femtosecond laser-induced water breakdown micro cavity fabrication in the (d) Laser focus scanning track for creating micro cavity in each layer of the SMSF in the .SMSF x-y plane. (e) A bird's eye view of a manufactured micro cavity was created

#### 5-Ayah Thabit Yahiya ,(2018)[57]

- **Fiber interferometer type :** Mach-Zehnder Interferometer (MZI)
- **Technique used:** weight effect
- **Fiber type:** arms of single mode –multimode –single mode
- **Wavelength:** tunability range (1554.721-1554.953) nm
- **Experimental result :** the Maximum tunability was obtained with two arms single mode –multimode –single mode (SMS-MZI) equal to(2.131 nm) and acceptable Phase shift was obtained with two arms multimode (MM-MZI)
- **Experimental and simulation work**

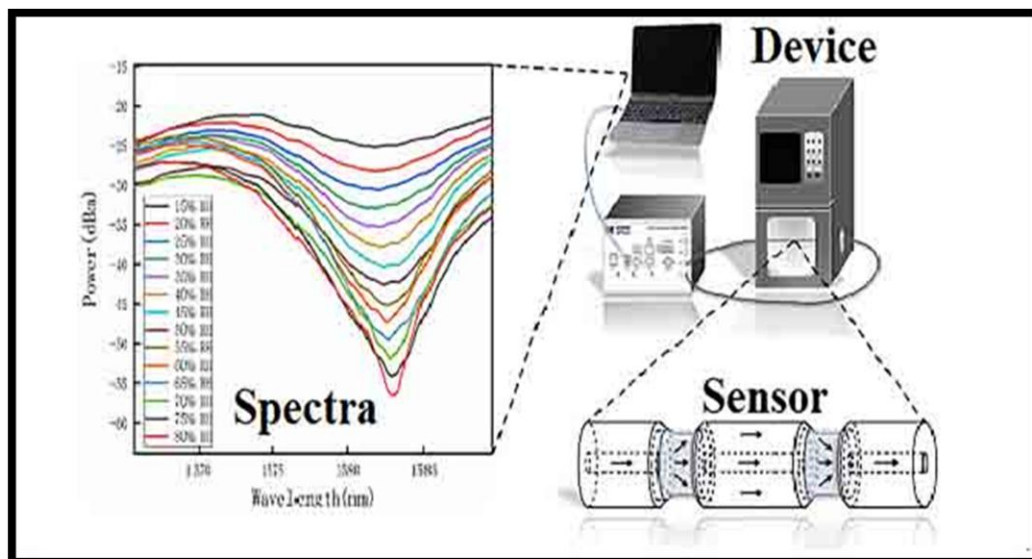
**6-XiaoliZhao<sup>a</sup>MingliDong<sup>b</sup>,FeiLuo<sup>a</sup> LianqingZhu ,(2019)[58]**

- **Fiber interferometer type :** Mach–Zehnder interferometer
- **-Technique used :** A fiber Bragg grating (FBG) is used in conjunction with an in-line Mach–Zehnder interferometer to create the sensor (MZI)
- **Fiber type:** thinned core fiber (TCF) (MMF)
- **-Experimental result :** Maximum sensitivity is 2.14 pm/, 35.2 pm/C, and 32.93 nm/RIU, respectively.
- **experimental and simulation work**

**7-Yufei Cheng; Wenhua Zhu; Rongxin Tong; Manli Hu; Tingting Gang (2020) [59]**

- **Fiber interferometer type: :** Mach–Zehnder interferometer
- **Technique used :** two sections of MMF are etched with hydrofluoric acid, then sodium alginate is coated on the corroded areas and immersed in calcium chloride solution to form calcium alginate (CaAlg)
- **Fiber type:** three sections of single mode fiber (SMF) and two sections of etched multimode fiber (MMF)
- **Experimental result :** While humidity is between 15%~80%, the sensitivity of the sensor can reach 0.48346 dB/%RH.

**Experimental work**



**Schematic diagram of an optical in-line SMF-MMF-SMF MZI for humidity sensing system**

# ***CHAPTER TWO***

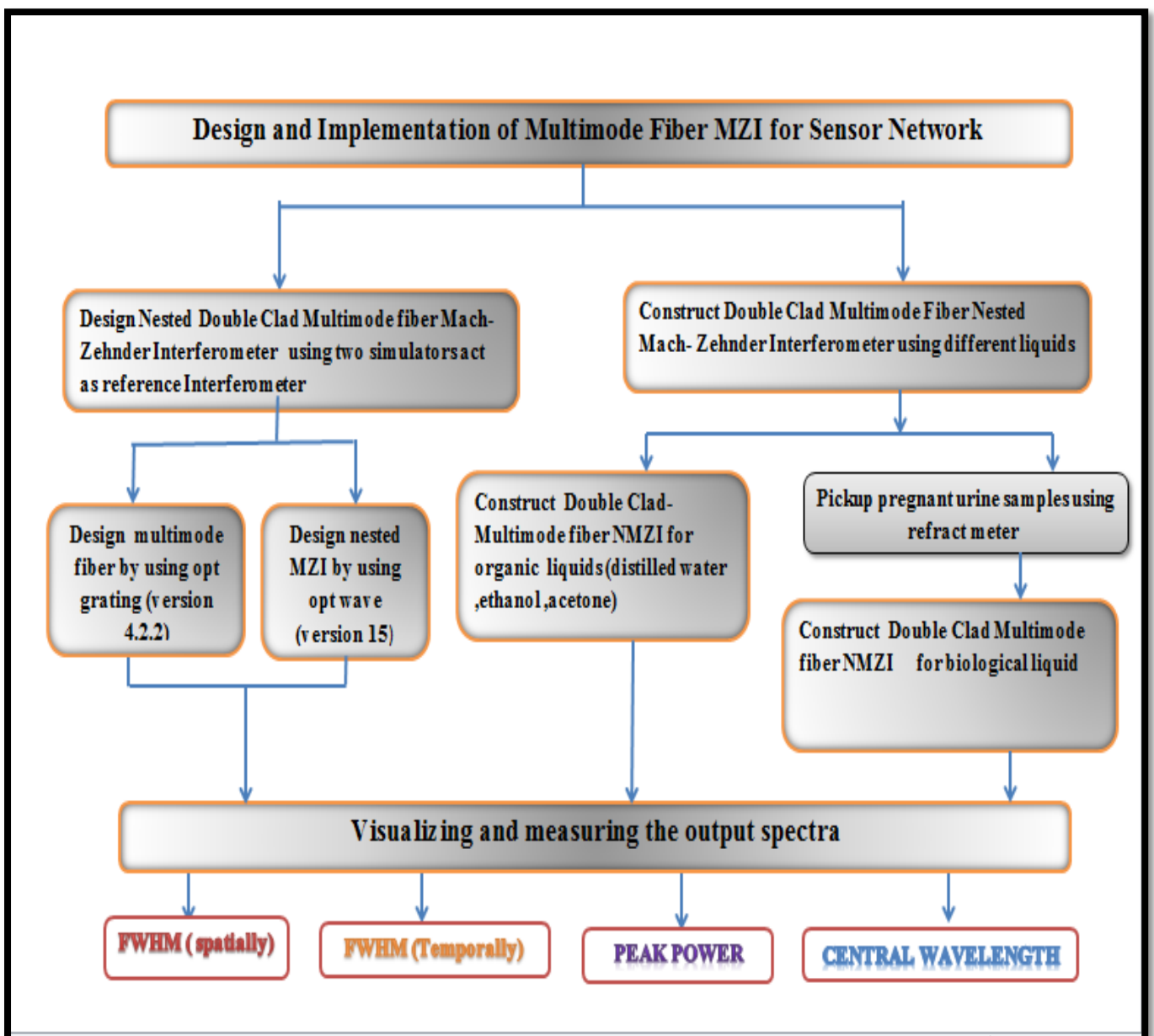
## ***Simulation and Experimental Setups***

# CHAPTER TWO

## Simulation and Experimental Setups

### Introduction

In this chapter optical sensor network system would be designed using opt grating (version 4.2.2)and opt wave version (15)after using Multimode Fiber – Nested Mach Zehnder Interferometer (DC-MMF-NMZI) and then constructed in the lab .This Scenarios was summarized as shown in Figure(2.1).



Fig(2.1) Scenarios of the work's steps

## 2.1 The Simulation Work

In these sections we using two simulators ,one for design etching multimode fiber by using opt grating Version (4.2.2).opt wave Version 15 was second simulator which using as virtual lab for nested design.

### 2.1.1 Etched Multimode fiber using opt grating

Double clad multi-mode optical fiber was designed using opt grating software, This was done by using a single-mode fiber .The parameters were changed to suitable to multimode fiber parameters. The RI of both core and cladding of MMF was selected according to standard fibers data sheet [60]. The multimode fiber core and cladding diameter were 50  $\mu\text{m}$ ,125 $\mu\text{m}$  respectively .Reducing amount of layers from cladding diameter was method to obtained double clad multimode fiber. Fig (2.2) shows the step of etching MMF

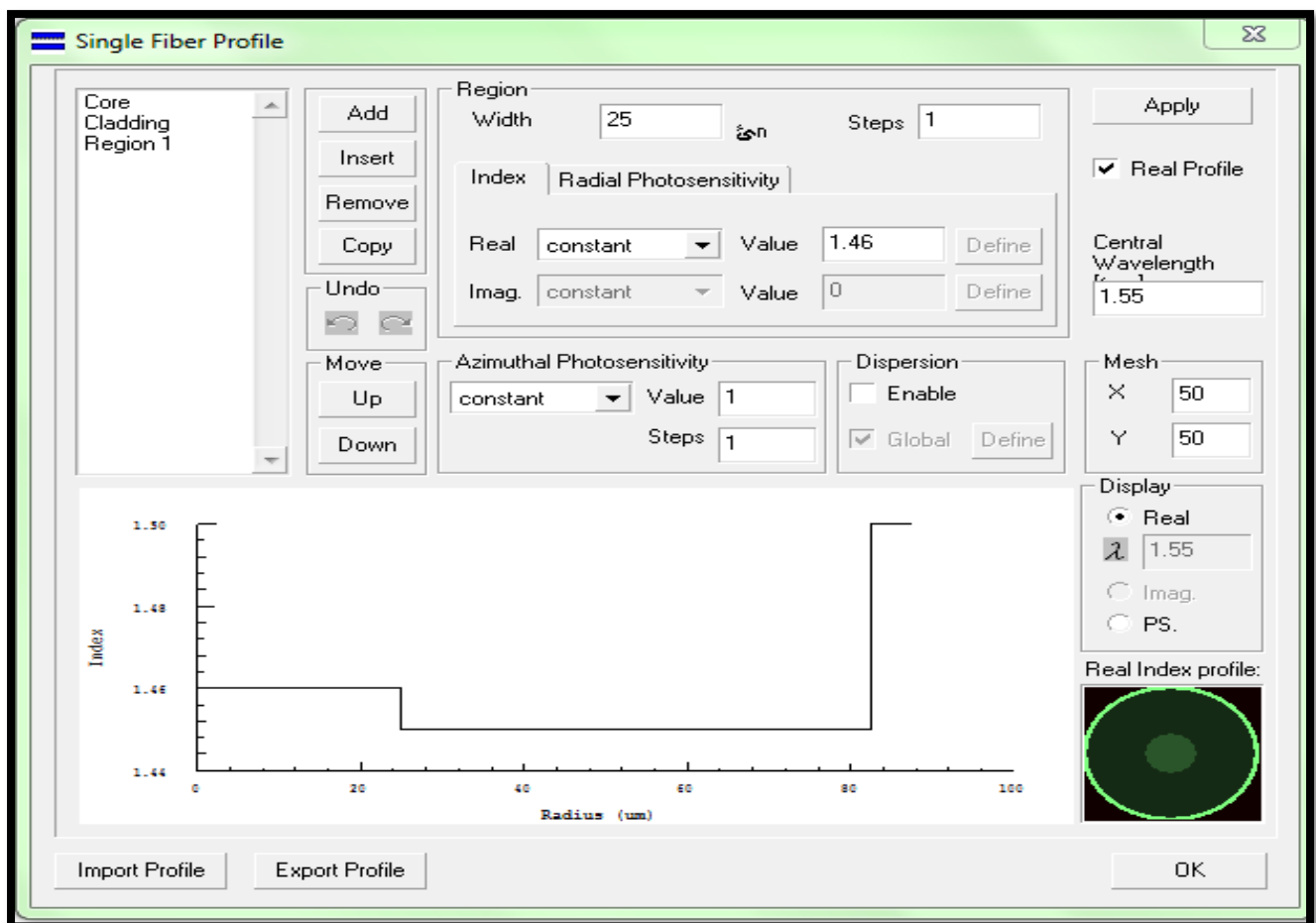
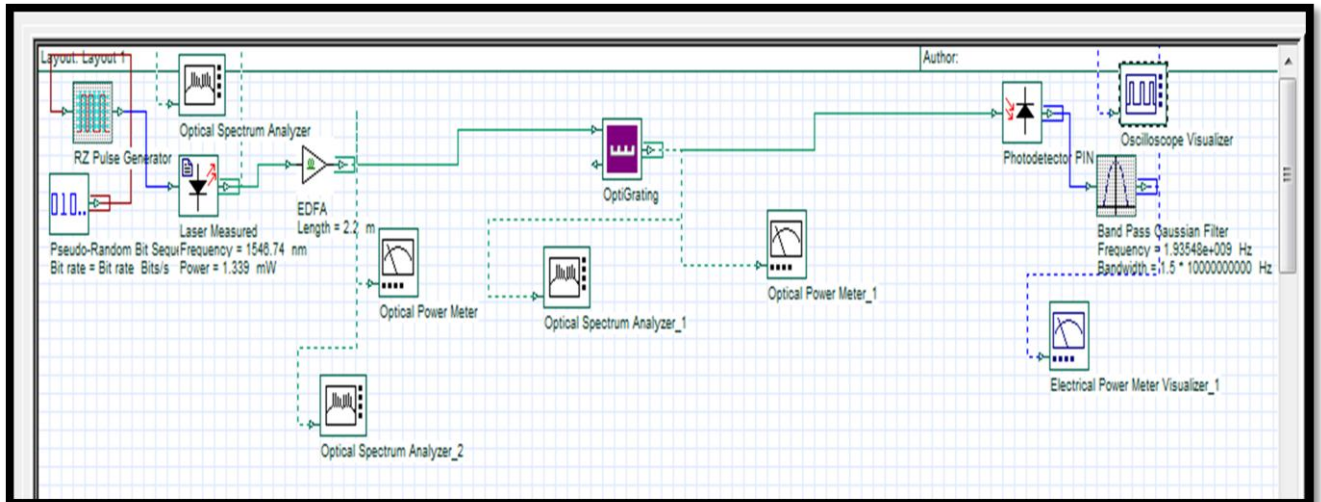


Fig (2.2) Etched MMF using optgrating

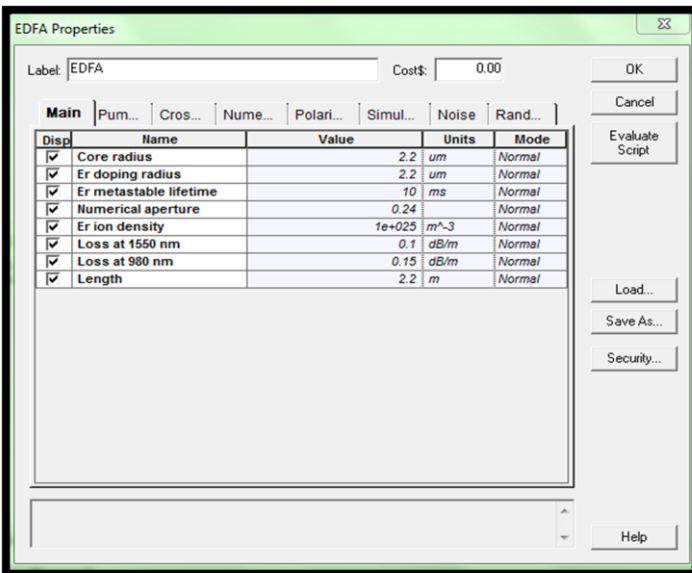


## 2.1.2 The design of nested Mach-Zehnder interferometer using opt system

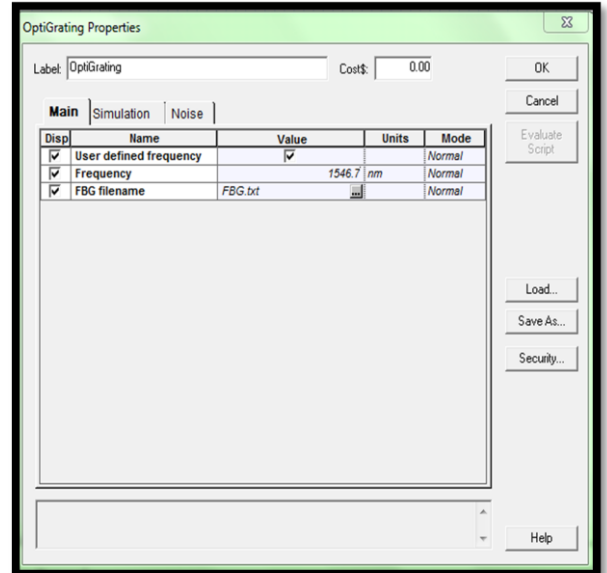
The simulation setup in Fig (2.3-a) consist of pulsed laser source, this source re design by simulation opt wave system 4.2.2 with center wavelength of 1546.74nm,10ns and 1.23m W [Appendix A] .The sensing head has been represented using opt grating component which was characterized as shown in Fig(2.3-b,c).



a



b



c

Fig (2.3) Simulation setup , a) Etched MMF MZI using opt wave , b)EDFA properties ,c)Opt grating properties

The Nested network was building using three levels of Double Clad MZI .First, 1:4optical power splitter was used to split laser beam input power between three MZIs' equally likely and the forth arm will be taken as an arm of comparison second, 4:1 coupler has been re combined three output signals. Erbium doped amplifier simulated to get 38.01 m W to satisfied nested condition as shown in Fig(2.4) .

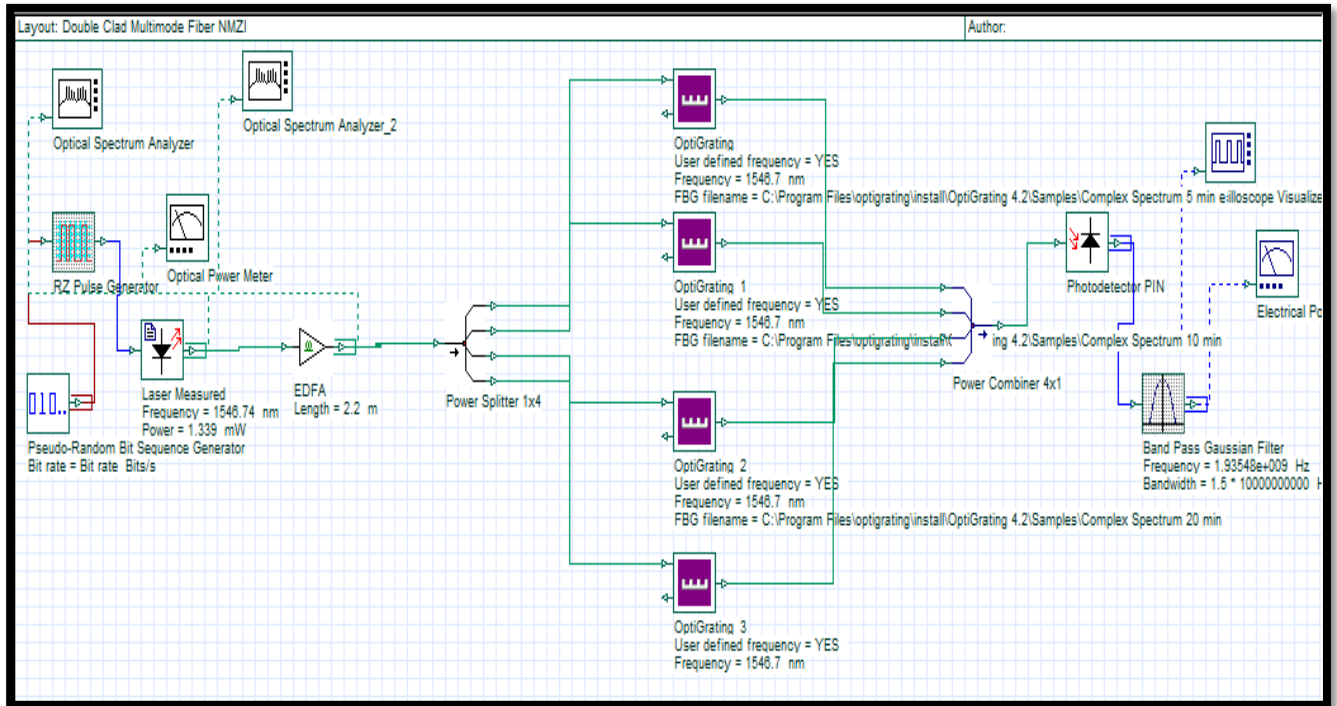


**Fig (2.4) simulation setup of NMZI**

## 2.2 Experimental work

Two experimental setups were performed using different fiber cladding diameter off MMF 118.7  $\mu\text{m}$ , 112.4  $\mu\text{m}$  and 72.5  $\mu\text{m}$ . The first with different refractive indices chemical liquids and the second setup with different refractive indices of biological samples . The optical components and devices in the experimental work will be presented in the following subsections as shown in Fig (2.5-a,b).

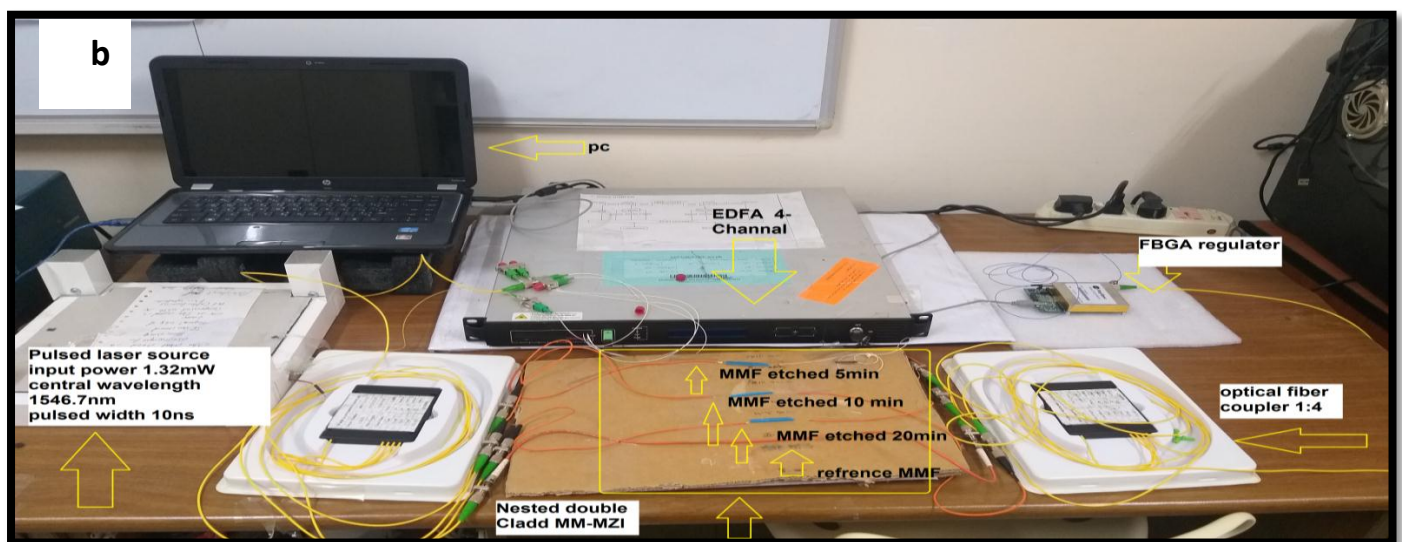
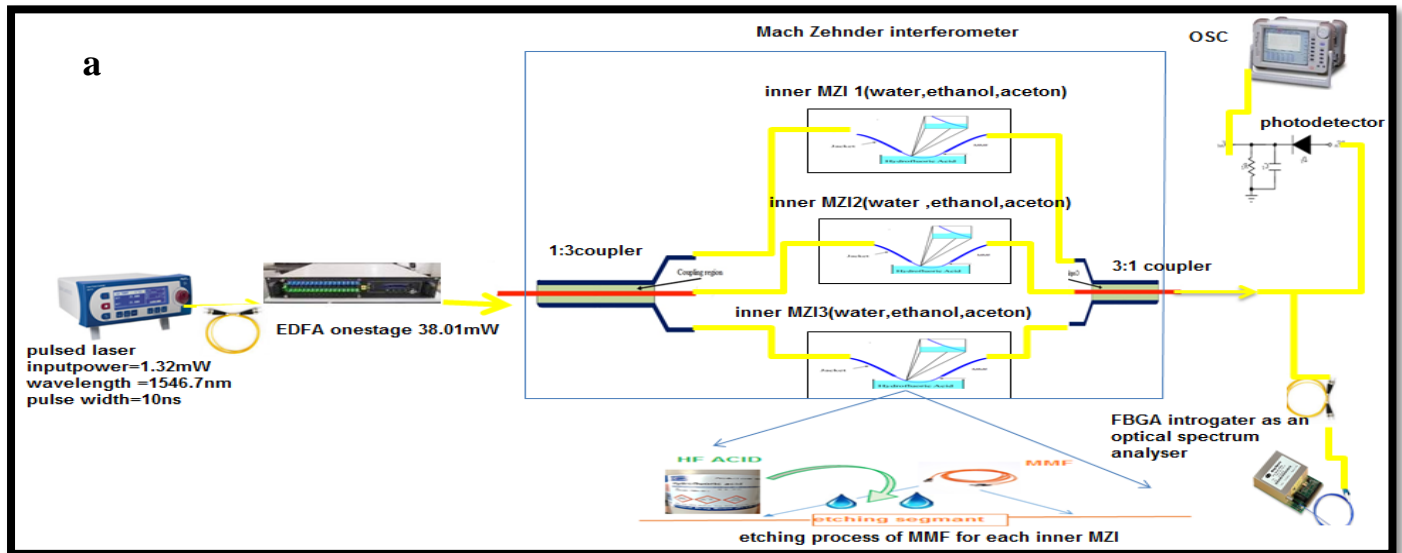


**Fig (2.5) DC-MMF NMZI with Chemical and Biological tests -a) The schematic diagram , -b)The experimental setup**

### 2.2.1 The Optical Laser Source

The implement low signal amplifier electronic circuit can convert the incoming pulse duration from 66  $\mu$ s to 10 ns. Narrow pulse generation could be achieved by controlling the voltage level above and below the lasing threshold of . The biasing resistor is used for controlling the electronically chop CW laser diode. after chopping this signal [61]. The new properties of laser used is illustrated in Table (2.1) and more detailed is shown in datasheet [Appendix A] .

**Table (2.1) Parameters for Pulse laser source**

<b>Parameter</b>	<b>Value</b>	<b>Unit</b>
Central Wavelength	1546.74	<b>Nm</b>
FWHM <sub>Temporal</sub>	10	<b>Ns</b>
FWHM <sub>Spatial</sub>	286	<b>Pm</b>

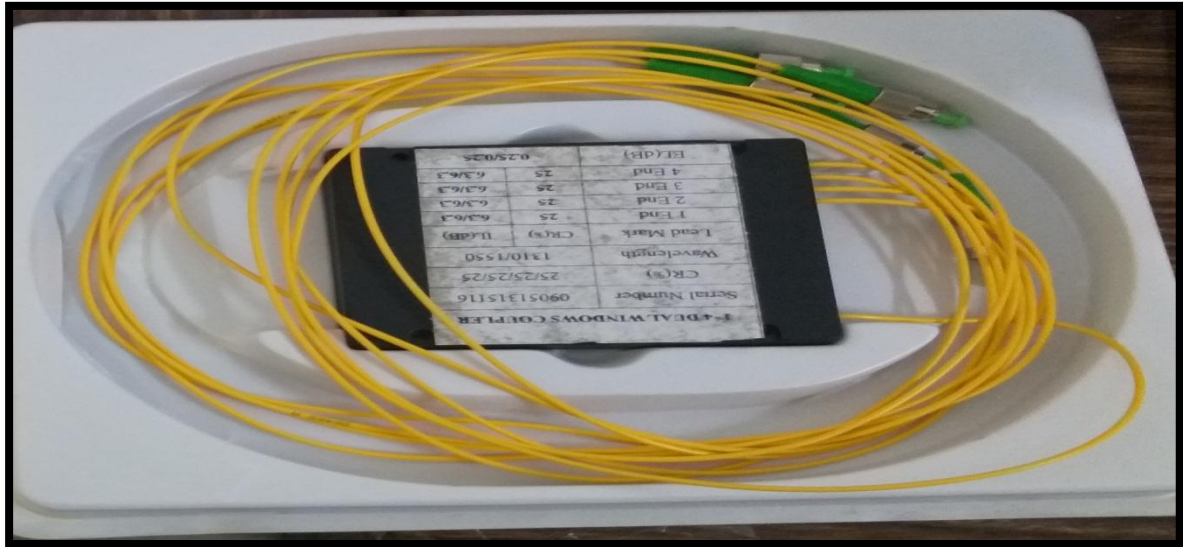
### **2.2.2 Erbium Doped Fiber Amplifier (EDFA)**

EDFA is an optical amplifier, gives 18 dBm gain for each of four channels which is in fact, generating a laser pumped by another laser with Erbium-doped fiber. Erbium-doped fiber amplifier (EDFA) is an important optical component .It supports low power optical signals and elevating it to the level where it is possible to stimulate Kerr effect. This component works as a Pump lasers ,Where it known as "pumping bands". Amplification occurs when there was an interaction between material and the phonons, which leads to vibrating all atomic in structures. In other hand an important factor is amplification rate . This rate is based on the range of optical wavelength amplified and it determined by the dopant ions' spectroscopic properties, the pump laser wavelength ,the source power and the ,optical fiber structure . Optical amplifiers work optically without converting from optical to electrical signals and back again [61]. For more information see [Appendix B].

### **2.2.3 Optical couplers**

In this work 1x4 WDM Dual-Window Fiber Optic Couplers are used . This types has been based on splitting input signals at wavelength range 1310 nm or 1550 nm equally, also it has  $\pm 40$  nm band width range and has coupling ratio 25.04 %. A maximum power of 1 W with connectors or fiber and 5 W needed couplers for spliced . The ranges bandwidth of this type of couplers are  $\pm 15$ nm,  $\pm 40$  nm for Narrowband also bandwidth around each center wavelength respectively. and a  $\pm 50$  nm or  $\pm 100$  nm

wideband couplers. Light wave Circuits (PLC) are used to combine optical signals. Its characteristics with circuit technology which provides a cost effective light splitting solution with small form factor, space saving product suitable to the ever changing networking requirements, high reliability also with its compact size, see [Appendix C]. In this work we will use 1×4, 1×3 WDM optical couplers as shown in Fig (2.6).



**Fig(2.6) Schematic of Optical Coupler**

## **2.2.4 Etched multimode fiber -Mach Zehnder interferometer**

### **2.2.4.1 Multimode fiber (MMF)**

Multi-mode optical fiber is a form of optical fiber that is mostly used for transmission signal for near distance. Its features is a comparatively floppy core diameter that allows many light modes to be transported but also limiting the extreme length of a transmission connection. Traditional 50 um core, 125 um cladding MMF type (OM2) was commonly used. These fibers readily supported applications ranging from Ethernet (10 Mbit/s) -(1 Gbit/s) and were suitable for use with LED transmitters due to their comparatively large core size. The optical specifications of MMF are presented in Table (2.2) [see appendix D]. Figure (2.7) shows the front view for the MMF fiber under microscope.



**Table (2.2) The optical specifications of MMF**

Parameter	Value	Unit
Operating $\lambda$ range	850/1310	n m
D-core	50	$\mu$ m
D- cladding	125	$\mu$ m
Dispersion	$1310 \leq 3.5$	[(ps/(nm*km))]

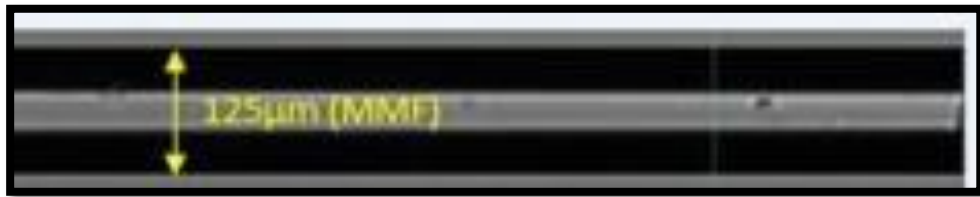


**Figure (2.7) Front view for the MMF fiber under microscope.**

#### **2.2.4.2 Etching process of MMF**

The standard multi-mode fiber 50/125 ( $\mu$ m) core to clad diameter size was immersed in HF acid of 40% concentration as shown in experiment setup Figure (2.8) . Because of its propensity to etch silicon synthesis hydrofluoric acid HF is a common used in research and industry .Aqueous inorganic acid solution fabrication of chips and electronics, mineral processing and glass etching are all examples of applications. Aside from its helpful features. In the silica pattern, the HF diffuses progressively as well. As a result, the modification in fiber mass can be chosen by assuming a dissolution rate that is dependent on the dissolution constant, the transfer surface area, and the acid concentration that cause dissolution as shown in Fig (3.8) and a MMF etching with different thickness under microscope were shown in Fig (3.9-a,b,c) .

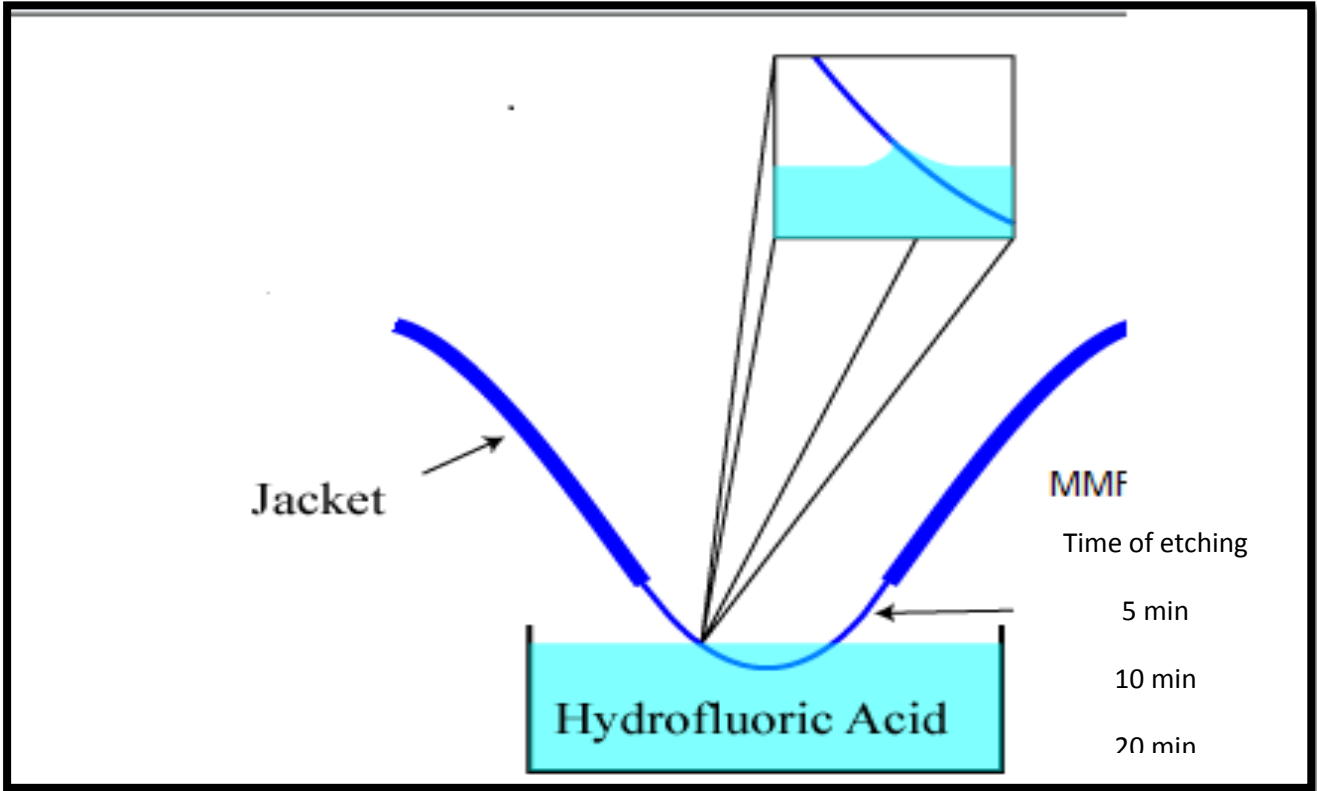
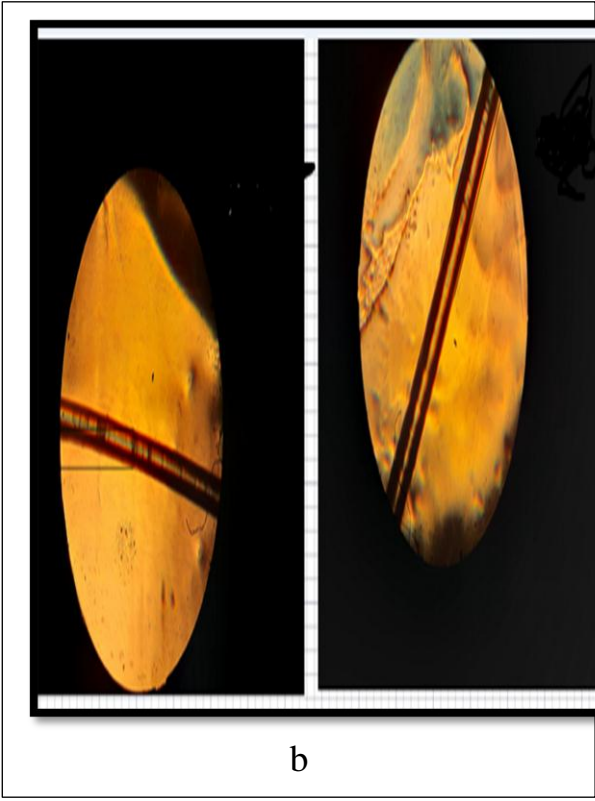
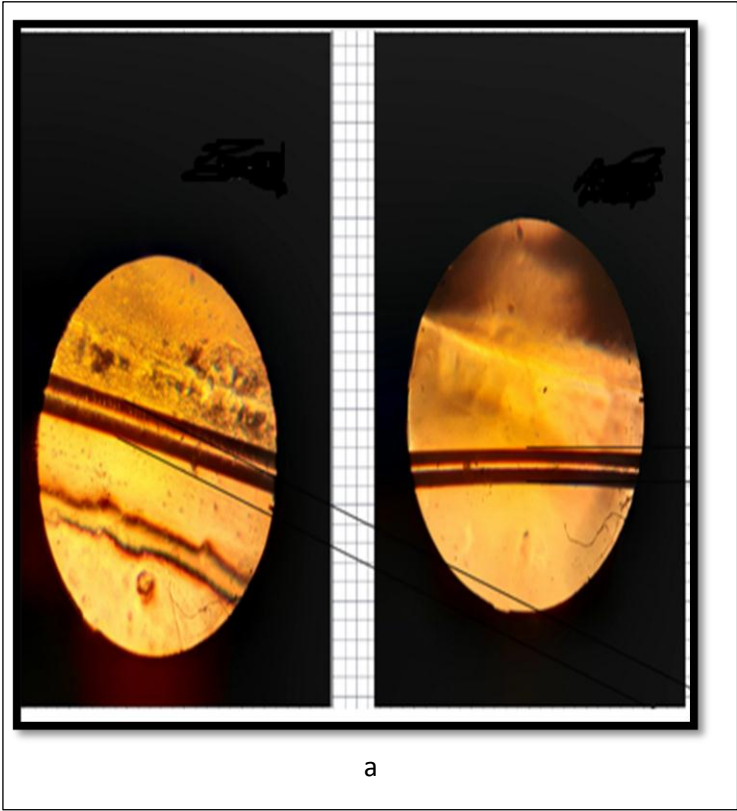
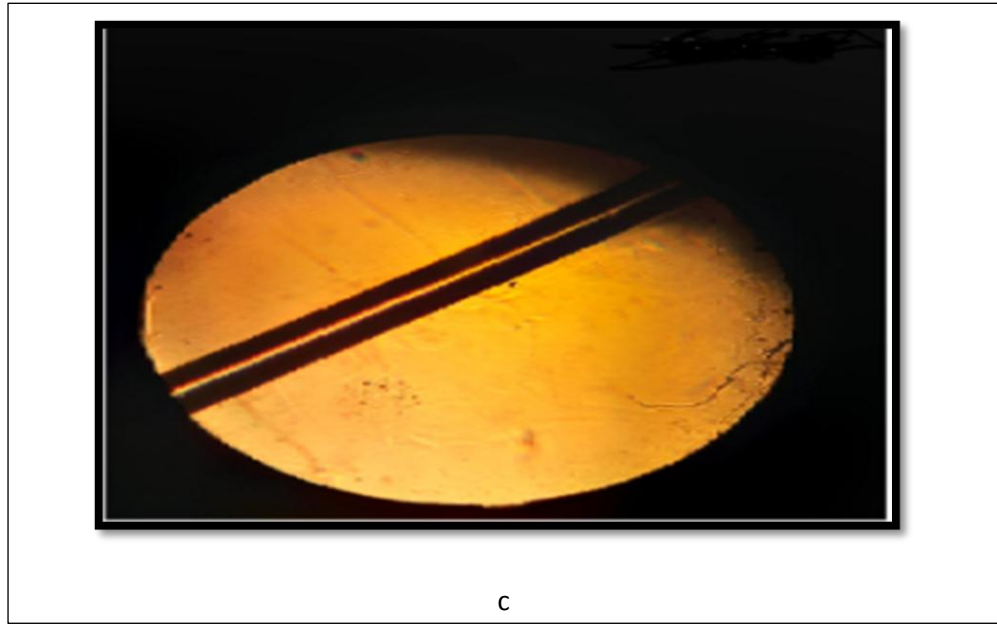


Figure (2.8) Etching process experiment set up



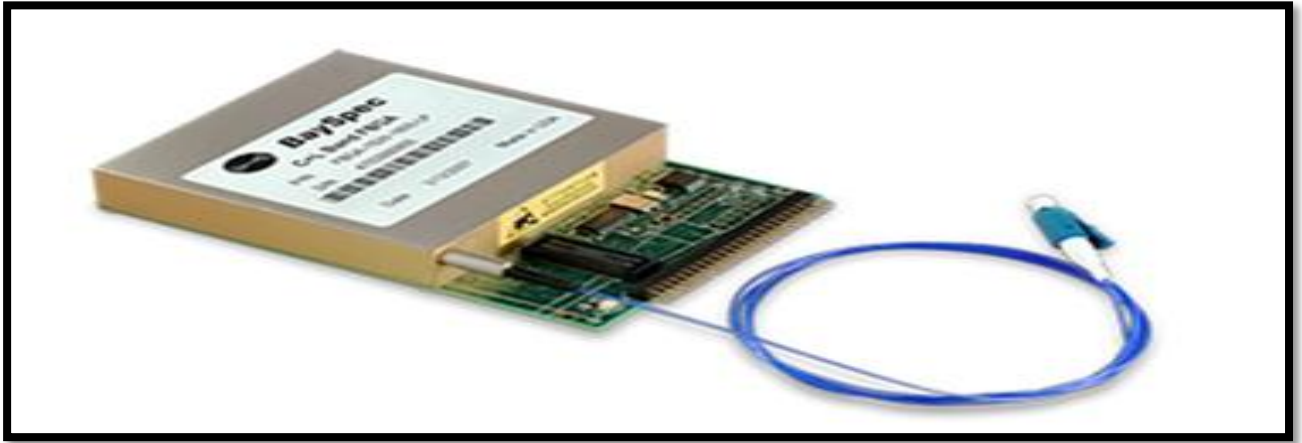


**Fig (2.9) MMF under microscope after etching (a)-5 min etching time and reminding fiber diameter 118.696  $\mu\text{m}$  ,(b)- 10 min reminding fiber diameter 112.3927 $\mu\text{m}$ , (c)- 20 min etching time and reminding fiber diameter and reminding fiber diameter 72.5321  $\mu\text{m}$**

### **2.2.5 Optical spectrum visualizer ( FBGA Interrogator (OSA))**

The optical signal was visualized by optical spectrum analyzer (OSA), it is a device that measures and displays the power distribution of an optical signal over a given wavelength range . The measuring parameters of this device are the detection window from 1525nm-1560 nm, Frequency response time 5 Hz , and Fixable wavelength range, allowed for single-mode, multimode and PCF fibers. OSA was used to monitor the interference spectra . Bay Spec Sense 20/20 Software Development Kit (SDK) supplies the interface for the software developer to access the Bay Spec Super Gamut TM and Nunavut TM series spectral engines. The Dynamic Link Library (DLL) in the SDK can be used under different programming environments: C, C++, Visual Basic and Lab VIEW. The SDK provides a set of functions that allow user to configure and control the spectral engines, acquire spectra and post-process the spectrum data. The OSA shown in Fig (2.10) having properties illustrated ,and more detailed in datasheet shown in [ appendix E].





**Fig(2.10)Optical spectrum analyzer FBGA interrogator**

### **2.2.6 Power Meter**

The power meter (FPM-300\FLS-300\FOT-300) that is used to measure the input and output of light source of 1550 nm wavelength in range C-band ,the detection power at the wavelength range 850,1310,1550nm and fiber coupled Fc connector ( see appendix F).

### **2.3 Chemical liquids**

In this section we will numerate the chemical liquids which has different refractive indices and it's optical properties ,these materials were applied on MMF –MZI etched section to construct double clad of MMF and study overall effects on the output properties .

#### **2.3.1-Distilled Water**

Distilled waters are a witch's ferment of dissolved and particulate particles. These solutes and particles have substantial optical properties and are very changeable in terms of type and concentration. As a result, natural waters' optical qualities vary greatly over time domain and frequency domain and never resemble those of clear water. The great variability of natural waters' optical properties is the distraction of those investigations accurate and simple computed data it is the connections between the biological, chemical

and geological constituents of natural water with optical properties as well as the substantial medium, that define the critical electromagnetic plane-wave propagation. [62]. The absorption spectrum shown in Fig (2.11)

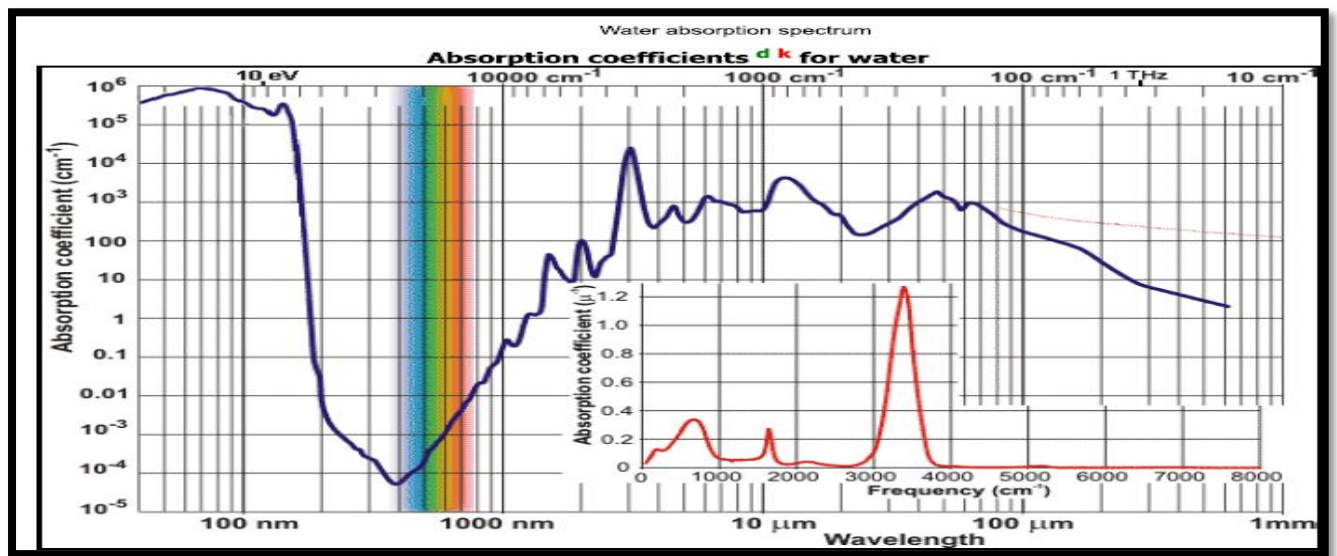


Fig (2.11) Optical Spectrum of Water[96]

### 2.3.2-Ethanol

Ethanol is a colorless, volatile, flammable, liquid with a distinctive odor. Ethanol chemical formula  $C_2H_5OH$  its chemical properties are listed in [Appendix G]. Ethanol properties listed in Table( 2.3), The absorption spectrum of ethanol is shown in Fig (2.12)

Table( 2.3) Ethanol properties [63,64]

Property	Value
Density	0.7893 g/cm <sup>3</sup> at 20 °C
Boiling point	78.24 ± 0.09°C
Refractive index (n) at 1546 nm	1.353 at 20° C
Viscosity	1.2mpa.s(at20° C)
Chromatic Dispersion (dn/dλ)	-0.010906 μm <sup>-1</sup>
Group Velocity Dispersion	GVD = 40.409 ps/(nm km)
Dispersion Formula	$n=1.349+0.00306\lambda^{-2}+0.00006\lambda^{-3}$

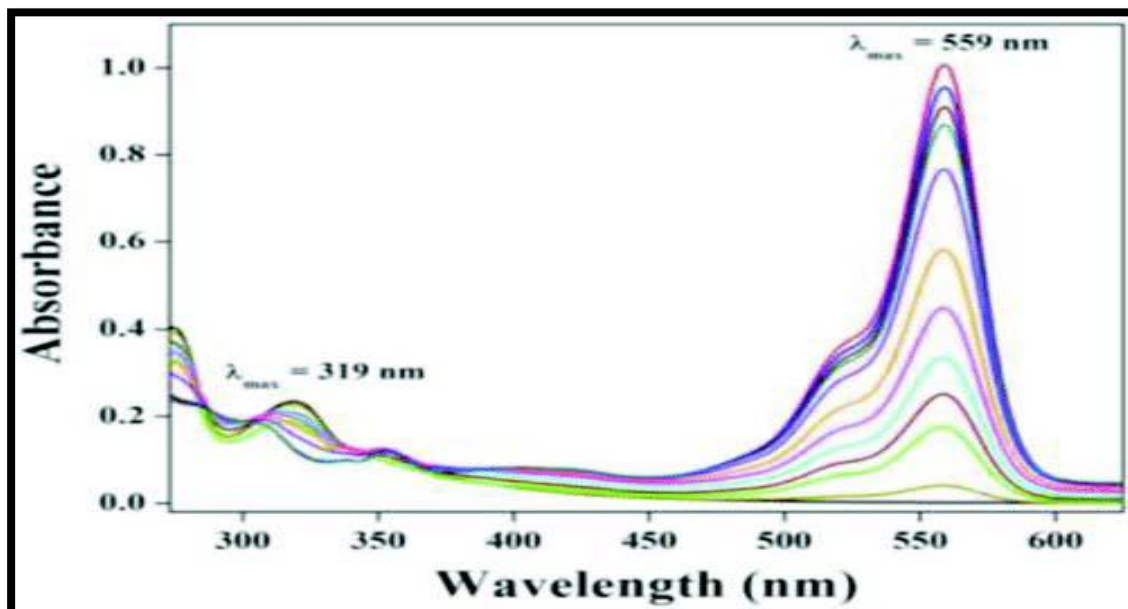


Fig (2.12) Absorption spectrum of ethanol [65]

### 2.3.3 Acetone

Acetone is a transparent clear colorless liquid with a fruity and sweetish odor has chemical formula is  $\text{CH}_3\text{-CO-CH}_3$  . Acetone chemical properties are listed in [Appendix H],and . Acetone properties are listed in table (2.4),Absorption spectrum of acetone is be shown in Fig (2.13)

Table (2.4) Optical properties of Acetone[66,67]

Property	Value
Density	0.7845 g/cm <sup>3</sup> at 20 °C
Boiling point	56.05 °C (132.89 °F; 329.20 K)
Refractive index (n) at 1546 nm	1.36 at 20 °C
Viscosity	0.36 cp (at 20 °C)
Chromatic Dispersion (dn/dλ)	-0.0103359 μm <sup>-1</sup>
Group Velocity Dispersion	GVD = 65.805 fs/(nm km)
Dispersion Formula	$n=1.349+0.00306\lambda^{-2}+0.00006\lambda^{-4}$

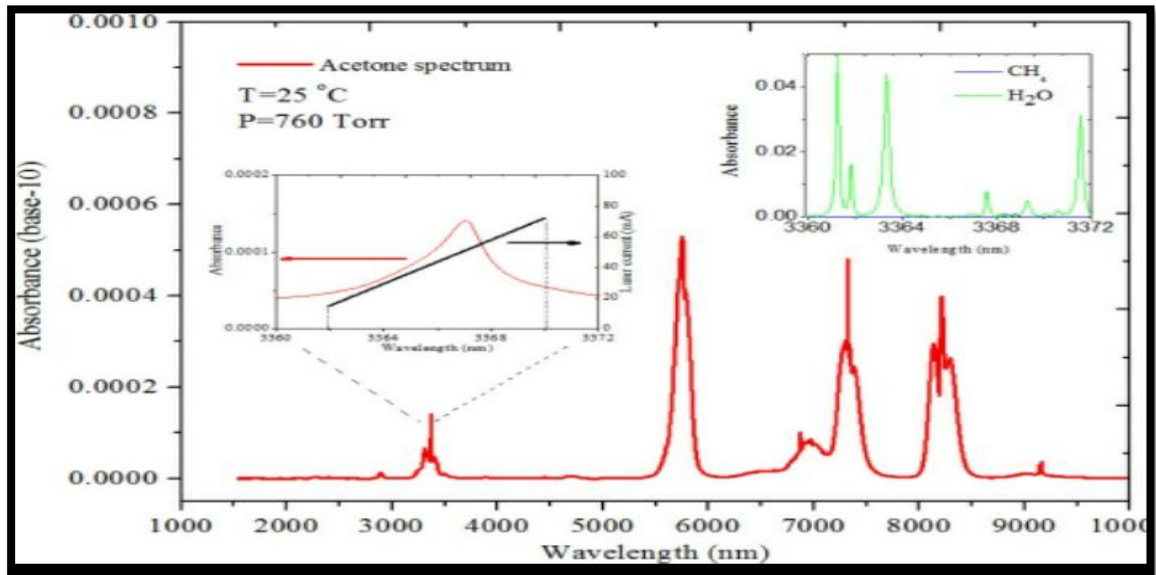


Fig (2.13) Absorption spectrum of acetone[67]

## 2.4 Refractive Index Measurement for Biological Samples

The refractive index of the urine samples was measured by PAL-BX/RI refract meter which has refractive index measuring range 1.3306 to 1.5284(5.0to 54C°) as shown in Fig (2.14) and see more details [Appendix I] .



Figure (2.14) Digital refract meter

***CHAPTER THREE***  
***Results, Discussion and***  
***conclusion***

# CHAPTER THREE

## *Results, Discussion, and Conclusions*

In this chapter, simulation and experimental results for Nested Mach-Zehnder interferometer using etched multimode fiber will be presented and discussed. Many affected parameters on the shape, pulse width and peak power of output pulse after using etched MMF-MZI are studied. The change in the central wavelength of etched MMF's and refractive indices that applied on the etched MMF cross section. Nested was used to test different refractive indices of biological and chemical liquids as a surrounding media to etching fiber section. The characteristic spectra (center wavelength, FWHM and transmission power) were measured by observing the shift occurs for the transmission spectrum. These results were taken under specific laboratory conditions and the room temperature was 25°C. This chapter we will discuss and analyze NMZI results in the following sections:

**3.1** Simulation and experimental results of design etched multimode fiber Nested Mach Zehnder Interferometer

**3.2** Experimental results of NMZI at chemical liquids .

**3.3** Experimental results of NMZI at biological liquids .

**3.4** Conclusions

**3.5** Future works

### 3.1 The results of simulation work .

Multimode fiber was etching using opt grating simulation Version (4.2.2) by reducing fiber thickness .As result in section 3.1.1 ,three fiber thickness were obtained from this simulation . In section 3.1.2 ,nested MZI was tested using opt wave simulation at different refractive indices .

#### 3.1.1 Simulation results of design etched MMF

Three different multimode fibers thickness have been designed using opt grating version (4.2.2)simulation . In this work , these multimode fibers ,the clad thickness is varied by reducing cladding layers gradually for 10,20,30  $\mu\text{m}$ . The modes distribution has been observed by this simulator as shown in Fig (3.1-a,b,c).

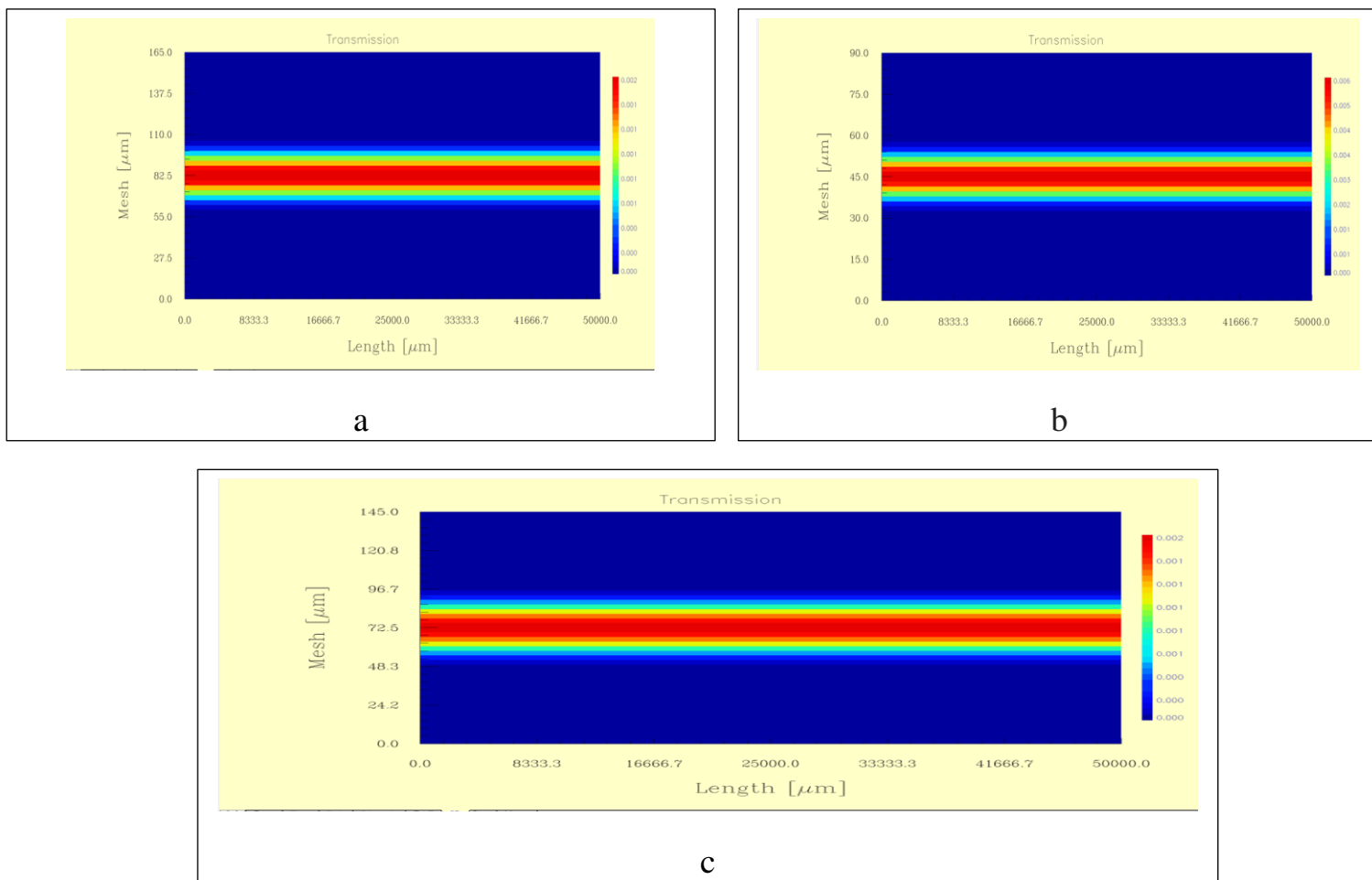


Fig (3.1) Simulation results to design MMF etching segment , a) for 5min ,b) for 10min ,c) for 20min

MMF has been designed by opt grating simulator and remove amount of cladding layers to obtain different fiber thickness 115,105,95  $\mu\text{m}$  . Fig (3.1) show that the red color is refer to the strength amount of power central in core, also the yellow color refer to the power less than peak power . Opt wave simulation was using as in section 2.1.2 with Fig (2.3-a) to obtain  $p_p$ ,  $\lambda_c$ , FWHM as shown in Table (3.1)

**Table (3.1 ) simulation results of etched MMF-MZI using Opt wave**

Etching time(min)	MMF thickness ( $\mu\text{m}$ )	Peak power of MZI ( $\mu\text{ W}$ )	$\lambda_c$ (nm)	FWHM (pm)
5	115	661.87	1546.75	156.56
10	105	638.25	1546.76	156.61
20	95	614.63	1546.78	156.65

From table (3.1) the effect of etching of cladding thickness was reducing in output power with respect to input power ,this because of index contrast which has been accrued in MMF etching cross section with length 5cm. The power was decreased with rough change in the central wave length .The output spectrum of etched MMF in Fig(3.2)

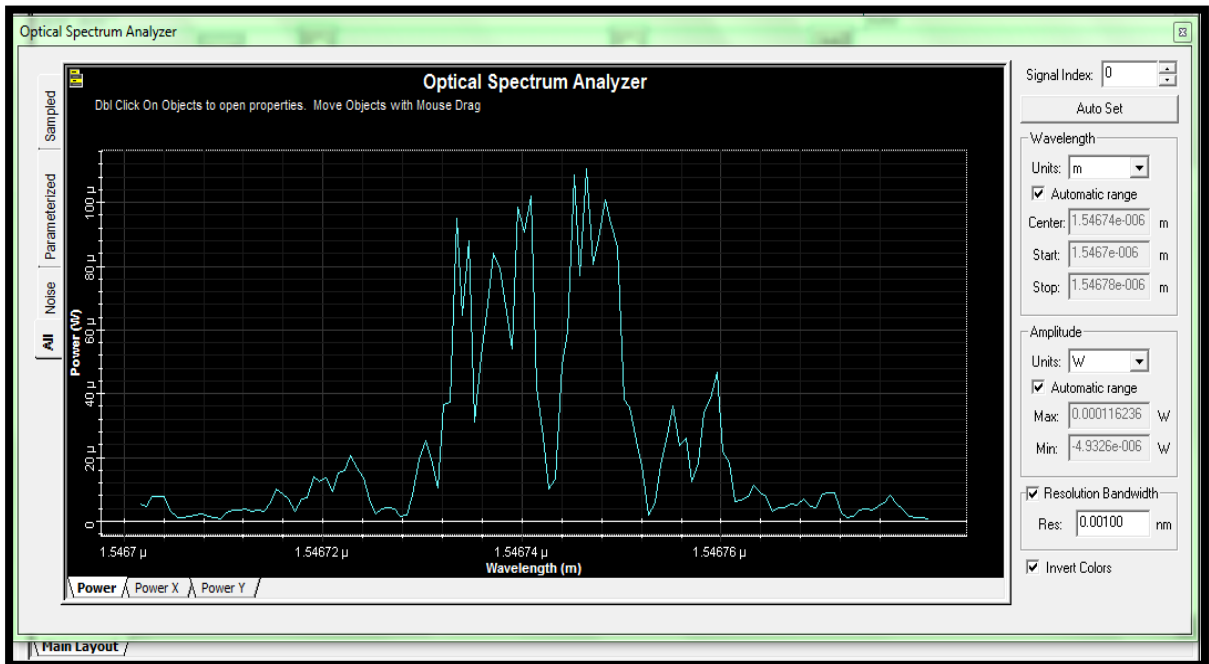


**Fig (3.2)Opt wave spectrum of etched MMF**



### 3.1.2 Simulation results of nested etched MMF-MZI

Nested was effected by the etching ratio for each fiber thickness .MMF with fiber 115  $\mu\text{m}$  connected nested the peak power has been reduced rapidly ,this mean the evanescent wave will be increasing . At MMF thickness 105  $\mu\text{m}$  and 95 $\mu\text{m}$  ,if we compared the nested MZI results with single MZI we found that the nested results more effective spatially FWHM more effect . high excitation to higher order modes play important role to reduce the output FWHM as shown in Table (3.2).

**Table (3.2) Opt wave result of nested etched MMF-MZI**

Time of etching(min )	MMF diameter $\mu\text{m}$	Nested Peak power ( $\mu\text{W}$ )	NMZI wavelength (nm)	FWHM (pm)
5	115	702.8	1546.73	90
10	105	356.3	1546.74	70
20	95	346.4	1546.738	40

### 3.2 Experimental results of the Characterization for the Pulsed Laser Source with MMF

pulse laser source was obtained of the output power 1.23mW , where the central wavelength of 1546.74 nm, full width at half maximum (FWHM) of 286 pm. This pulsed laser source is performed to operate at pulse duration of 10 ns as illustrated in Fig(3.3).

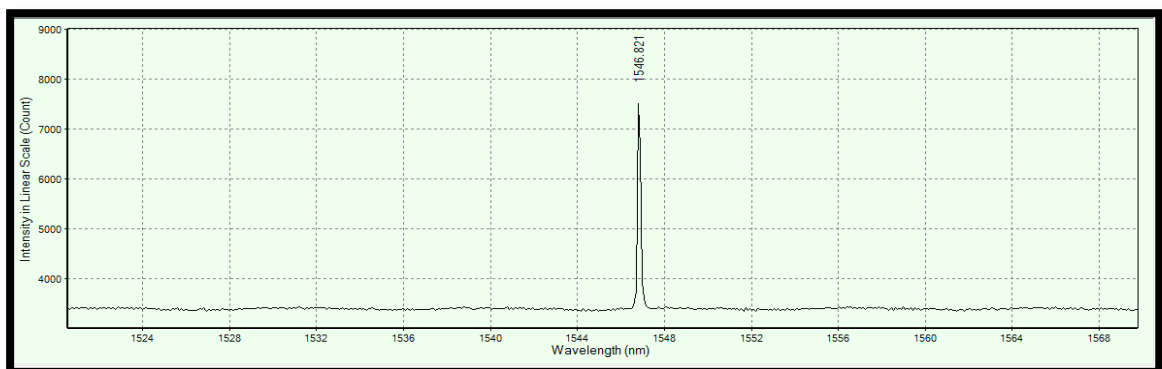


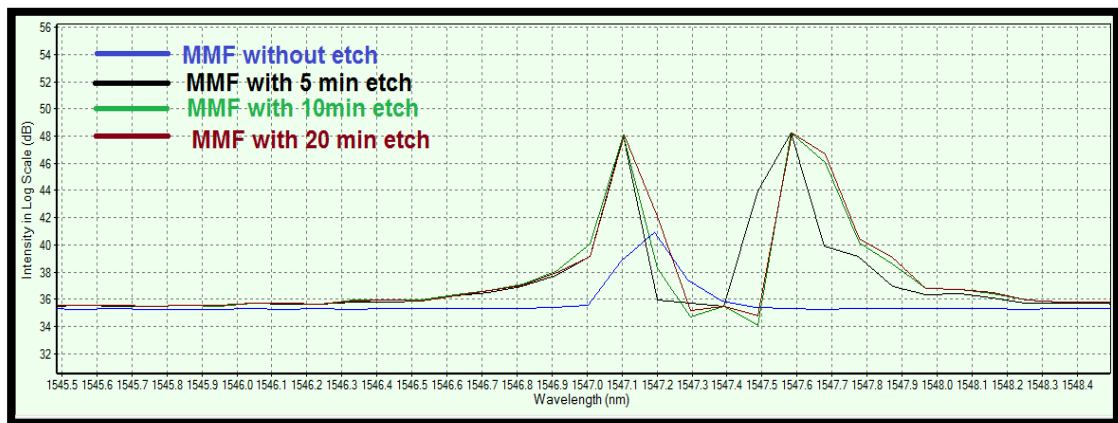
**Fig (3.3) pulse laser source spectrum visualized with FBGA**

In Fig(3.3) the value of the wavelength has been shifted to become 1547.18nm also decreases in the peak power value was observed 48.8 $\mu$ W . Experimentally, multi-mode fiber has been etched by removing varying numbers of layers of the cladding using chemical etching method by hydrofluoric acid with a concentration of 40% for a period of 5, 10 and 20 min. The pulsed laser source with the characteristics before was applied on the multi-mode optical fiber as illustrated in Table (3.3) .

**Table (3.3) Experimental results of etched MMF-MZI**

Time of etching(min)	MMF diameter ( $\mu$ m)	Peak power ( $\mu$ W)	$\lambda_c$ (nm)	FWHM ( $\mu$ m)
5	118.7	445.76	1547.10	130
10	112.3	186.33	1547.09	174
20	72.5	188.23	1547.07	203

From Fig(3.4) shown below the effect of multimode fiber etching are observed of 5,10,20 min compared with same fiber but without etching .The wavelength shifting at these cases has been obtained clearly especially at case 5min etch .



**Fig(3.4) Etched MMF compare with pulse laser source spectrum visualized with FBGA**

### 3.3 Experimental results of linear test NMZI for chemical liquids

Experimentally different chemical liquids material were used different with refractive indices on etched MMF segment . Each sample was testing for 5min,10min,20 min with input power of 1.23 mW . From Table (3.4) the wavelength shifting was obtained

according to different fiber thickness .This different fiber thickness in addition to change in refractive index of surrounding media caused decreasing in output power and FWHM. Maximum wavelength shifting was obtained in the case of 20min with fiber diameter 72.5 $\mu$ m. In ethanol liquids rapid detection were found at FWHM of 292 pm. Double peaks were appeared almost in case of 20 min for all refractive indices.

**Table (3.4)Experimental results of etched –MMF-MZI at using chemical liquids**

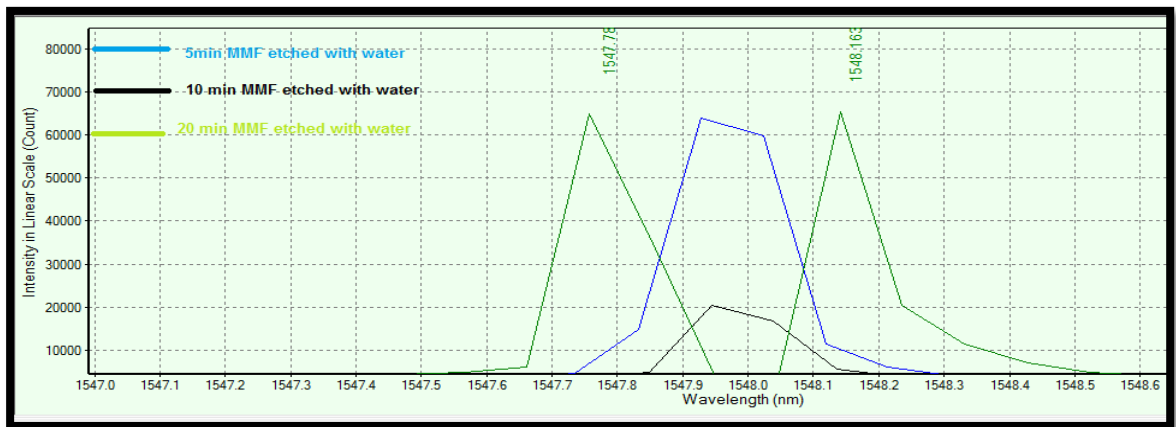
<b>Material</b>	<b>Time of etching(min)</b>	<b>MMF diameter <math>\mu</math>m</b>	<b>Peak power <math>\mu</math>W</b>	<b><math>\lambda_c</math> nm</b>	<b>FWHM pm</b>
<b>Distaled Water 1.317</b>	<b>5</b>	<b>118.7</b>	<b>918.19</b>	<b>1547.97</b>	<b>192</b>
	<b>10</b>	<b>112.9</b>	<b>281.9</b>	<b>1547.98</b>	<b>196</b>
	<b>20</b>	<b>72.5</b>	<b>905.5</b>	<b>1547.78</b>	<b>135</b>
			<b>884.3</b>	<b>1548.16</b>	<b>107</b>
<b>Ethanol 1.352</b>	<b>5</b>	<b>118.7</b>	<b>922.87</b>	<b>1547.88</b>	<b>286</b>
			<b>878.30</b>	<b>1548.01</b>	<b>292</b>
	<b>10</b>	<b>112.9</b>	<b>720.18</b>	<b>1547.93</b>	<b>262</b>
	<b>20</b>	<b>72.5</b>	<b>1048.85</b>	<b>1547.66</b>	<b>164</b>
<b>1221.12</b>			<b>1548.24</b>	<b>158</b>	
<b>Acetone 1.358</b>	<b>5</b>	<b>118.7</b>	<b>799.6</b>	<b>1547.96</b>	<b>161</b>
			<b>842.97</b>	<b>1547.78</b>	<b>113</b>
	<b>10</b>	<b>112.9</b>	<b>999.09</b>	<b>1548.17</b>	<b>79</b>
			<b>169.68</b>	<b>1548.31</b>	<b>365</b>
			<b>996.63</b>	<b>1547.70</b>	<b>153</b>
<b>20</b>	<b>72.5</b>	<b>834.11</b>	<b>1548.23</b>	<b>140</b>	

From table(3.5) water and ethanol were behaved differently from other liquid substances , Since both liquids showed a double-peaked sign in their results at the wavelength range (1547.23-1548.23)nm ,also the maximum  $\Delta\lambda_c$  was obtained at case of ethanol NMZI.

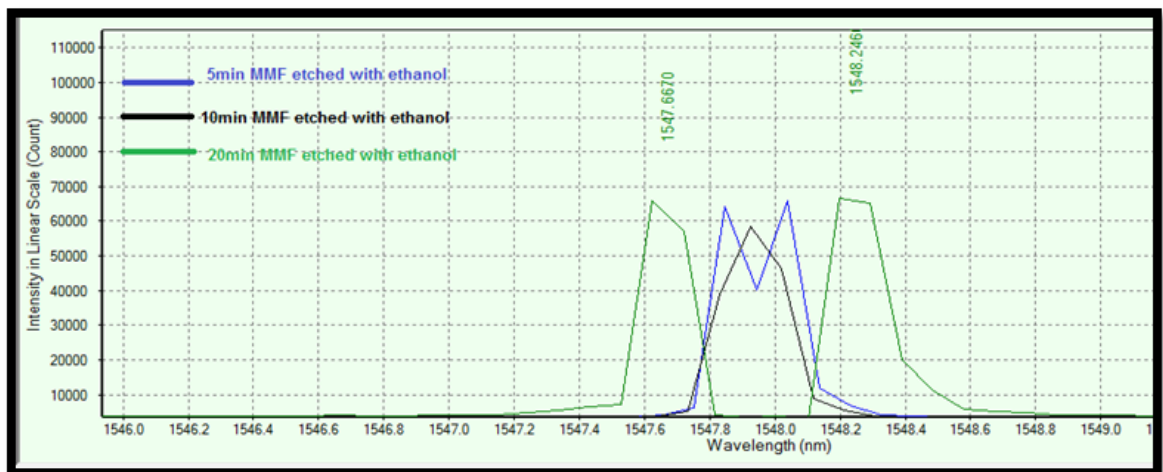
**Table (3.5) Experimental results of NMZI using chemical liquids**

Chemical liquids	Central wavelength (nm)	Peak power ( $\mu$ W)	FWHM spatially(pm)	FWHM temporally(ns)	Compression factors	$\Delta\lambda$ (nm)
<b>Water</b> <b>1.317</b>	1547.59	66.53	89.7	11.14	0.31	0.89
	1547.88	58.55	100.8	9.92	0.35	1.186
<b>Ethanol</b> <b>1.352</b>	1547.23	66.77	209	4.74	0.73	0.539
	1548.23	59.30	208	4.76	0.72	1.626
<b>Acetone</b> <b>1.358</b>	1547.95	64.99	140	7.14	0.48	1.25

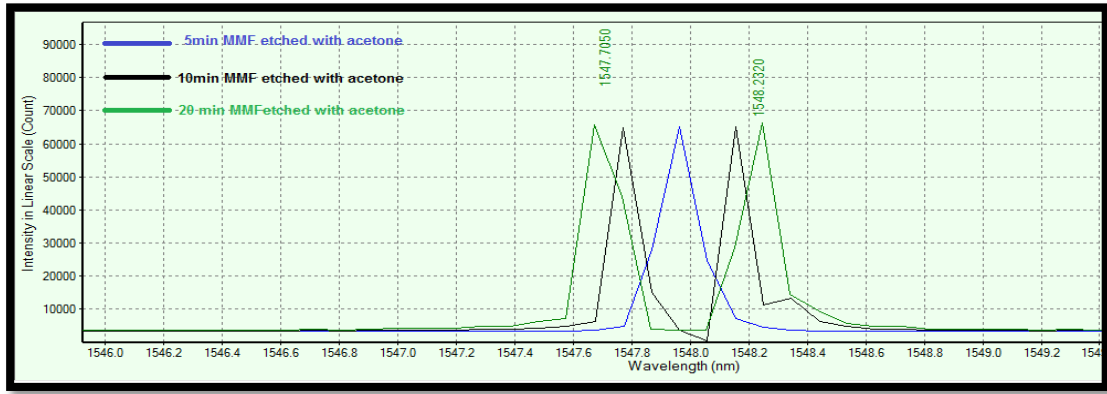
Fig (3.5-a,b,c) show NMZI for three different material each one is nested for three different fiber thickness.



a



b



C

**Fig (3.5)Output spectrum of NMZI for three different fiber diameter ,a) for distilled water, b)for ethanol ,c) for acetone**

The relationship of wavelength with the refractive index of three different liquids materials as shows in Figure (3.6) .

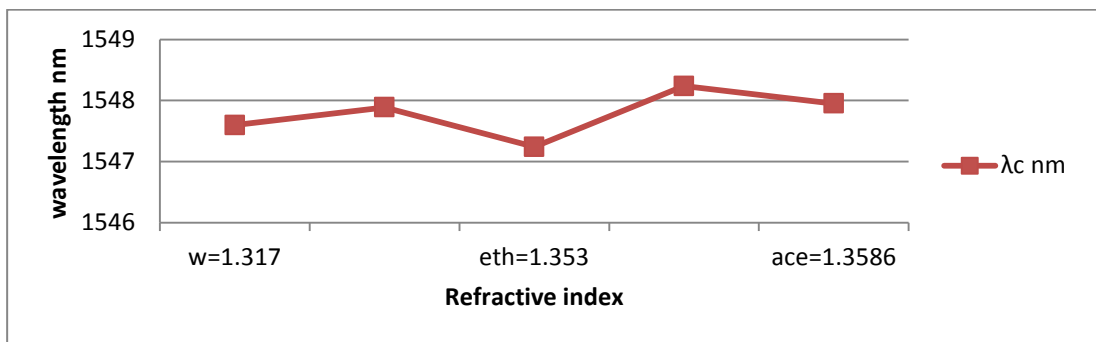


**Fig (3.6) Relationship between NMZI wavelength and three different refractive indices of liquids**

### 3.4 Experimental results of etched MMF-MZI at biological liquids .

Three pregnant patient urine samples refractive indices were measured using digital refract meter ,these values illustrated in Table(3.6)

**Table (3.6) Refractive indices of pregnant patient urine samples**

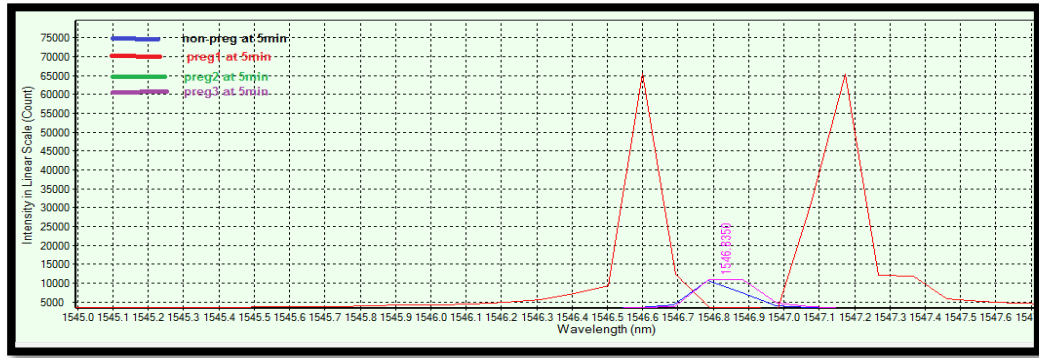
Case of patients	Refractive Index
Patient 0(non -pregnant)	1.34005
Patient preg 1	1.34235
Patient preg 2	1.34135
Patient preg 3	1.34123

Three pregnancy samples were tested by using etched MMF-MZI to improve the sensitivity ability of sensor network .the different pregnancy urine samples refractive indices were effected as double clad , simultaneous detection and sensing of refractive index with respect to varied fiber thickness were obtained .These refractive indices were proven the efficiency of etched segment for MMF, in addition to the possibility of reusing the same fiber for different cases as illustrated in Table (3.7)

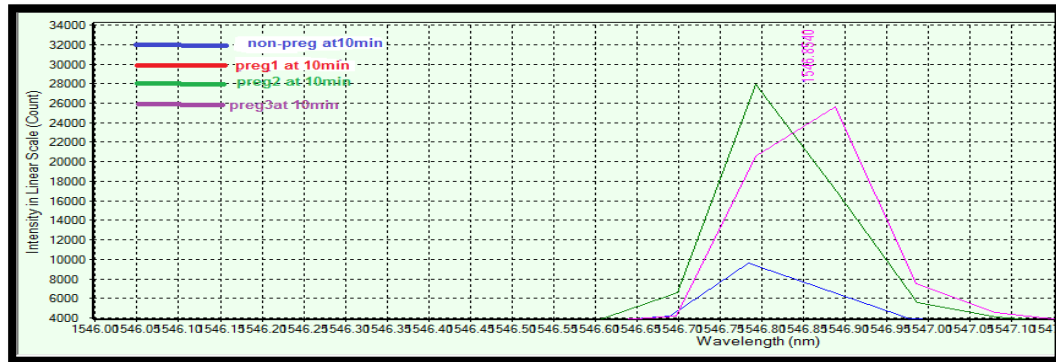
**Table (3.7) Experimental results of etched–MMF-NMZI at using urine pregnancy samples**

patients	Etching time(min)	Measured nested parameters			Calculated nested parameters		
		Po $\mu$ W	$\lambda$ c (nm)	FWHM (pm)	CF	Normalized frequency(V)	Number of modes
<b>Non-pregnant</b> 1.3405	5	139.5	1546.804	230	0.45	143	10190
	10	124.1	1546.803	243	0.84	122	7506
	20	100.4	1546.51 1547.12	135 176	0.94	88	3932
<b>pregnant 1</b> 1.34135	5	832.3 866.6	1546.60 1547.15	115 143	0.45	144	10841
	10	47.15	1546.95	32	0.11	147	10374
	20	116.2 839.3	1546.53 1547.24	152 147	0.522	29	416
<b>Patient 2</b> 1.34235	5	628.6	1546.81	60.16	0.65	146	10863
	10	374.6	1546.81	317	1.108	145	10473
	20	429.8	1546.83	189	0.66	64	2047
<b>Patient 3</b> 1.34123	5	153.9	1546.85	237	0.82	145	10791
	10	354.8	1546.87	196	0.68	143	10170
	20	375.7	1546.90	195	0.67	90	4053

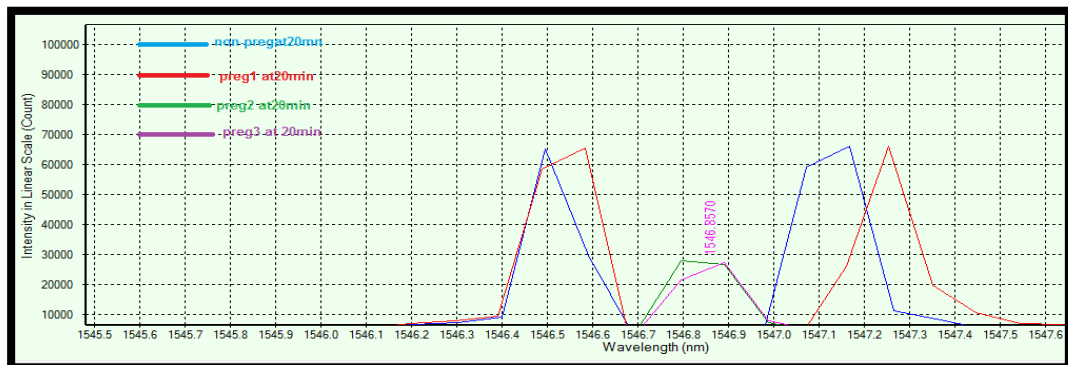
The higher peak power will be obtained in case of 10min etching at fiber diameter of 112.9 $\mu$ m for urine samples, also the phase shift was varied simultaneously with refractive index of urine samples and MMF cladding thickness. Nested parameters for urine pregnancy samples have been calculated using eq.(1.5),(1.6),(1.7),(1.8). Figure (3.7-a,b,c)shows the phase shift between three pregnant samples compared with reference sample ,non-pregnant .The effect of refractive index change was appeared in these result .



a



b



c

**Fig (3. 7) peak power spectrum of three pregnant samples with compared with non-pregnant at fiber, a) at fiber diameter 118.69  $\mu\text{m}$ , b) at fiber diameter 112.3927  $\mu\text{m}$ , c) at fiber diameter 72.532  $\mu\text{m}$**

Maximum value of FWHM has been obtained at NMZI, each pregnant sample was tested by nested for each thickness at the same time. In results of the  $P_o$ ,  $\lambda_c$ , FWHM were obtained with the simultaneous variance in the refractive index and cladding thickness, at input power amplified by 38.01 mW using EDFA, as shown in Table (3.8).

**Table (3.8) The results of NMZI parameters**

Refractive indices	P <sub>o</sub> (NMZI) μW	λ <sub>c</sub> ( nm)	FWHM (pm)
<b>1.34235</b>	7.873	1546.821	<b>283</b>
<b>1.34135</b>	7.514	1546.820	<b>267</b>
<b>1.34123</b>	7.66	1546.851	<b>333</b>

The effect of RI of pregnancy urine samples and non-pregnancy on the etching MMF among NMZI has high phase shift ,FWHM. These different values gave us an indication about ability of NMZI to distinguish between multi samples (refractive indices) with same fiber (reusable).The following figure show four samples have investigated using nested MZI as shown in Fig (3.8).

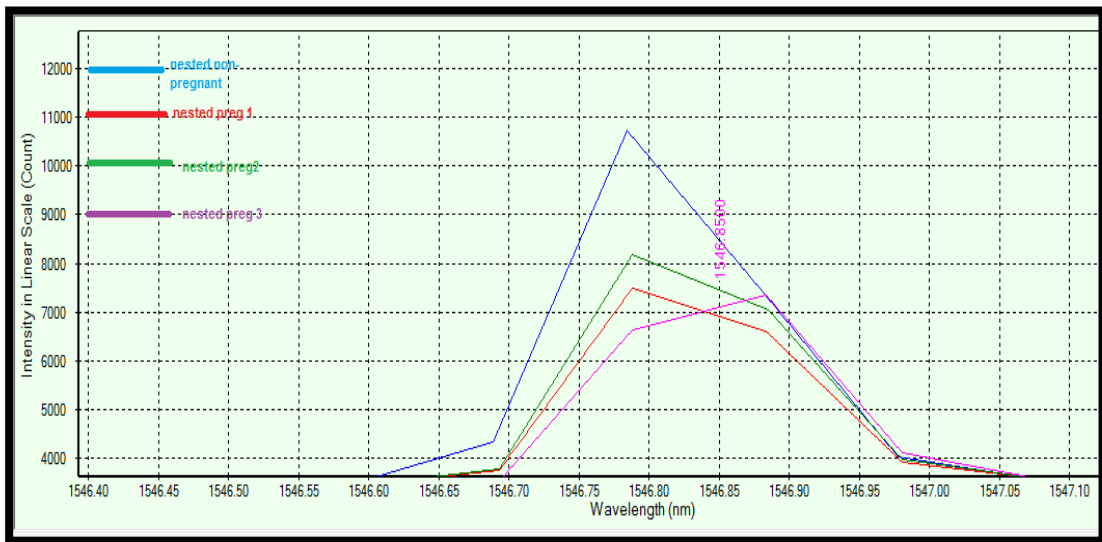


**Fig (3.8) The peak power of nested DC-MMF NMZI (urine pregnancy1,2,3 samples)compared with nested non-pregnant**

### 3.5Conclusions

From the obtained results ,the rapid detection was improved in case of nested Mach Zehnder interferometer at FWHM of 209 pm of ethanol liquid .Reusable sensing head was proved and efficient ability to distinguish between multi different refractive indices (signals)



### **3.6 Future works**

- 1.Design NMZI using femtosecond laser source +--+ .
- 2.Design NMZI using photonic crystal fiber .
3. Using double clad PM fiber to construct Nested Mach-Zehnder interferometer for detection and sensing .
4. Using double clad FBG fiber to construct Nested Mach-Zehnder interferometer for detection and sensing network.
5. Using double clad PM fiber and FBG to construct hybrid Mach-Zehnder interferometer.
6. Using hollow core fiber to construct Mach-Zehnder interferometer.
- 7.Obtain the ratio power clad to power core for different In line fiber MZI using comsol multiphysics .

# REFERENCES

## References

- [1] Wenchao LI , Yonggui YUAN , Jun YANG, and Libo YUAN , " Review of Optical Fiber Sensor Network TechnologyBased on White Light Interferometry" *PHOTONIC SENSORS* ,Vol. 11, No. 1, pp 31–44 ,(2021)
- [2] D. Liu, Q. Sun, P. Lu, L. Xia, and C. Sima, “Research progress in the key device and technology for fiber optic sensor network,” *Photonic Sensors*, Vol 6, No 1, pp 1-25 ,(2016)
- [3] Y. Wang, J. Gong, D. Y. Wang, B. Dong, W. Bi, and A. Wang, “A quasi-distributed sensing network with time-division-multiplexed fiber Bragg gratings,” *IEEE Photonics Technology Letters*, Vol 23 ,No 2 ,pp70–72 ,( 2011)
- [4] Z. Wang, F. Shen, L. Song, X. Wang, and A. Wang, “Multiplexed fiber Fabry-Pérot interferometer sensors based on ultrashort Bragg gratings,” *IEEE Photonics Technology Letters*, Vol 19 ,No 8 , pp 622–624. ,(2007)
- [5] K. Stępień, M. Slowikowski, T. Tenderenda, M. Murawski, M. Szymanski, L. Szostkiewicz, *et al.*, “Fiber Bragg gratings in hole-assisted multicore fiber for space division multiplexing,” *Optics Letters*, Vol 39 ,No 12 , pp 3571–3574 (2014)
- [6] J. Huang, X. Lan, M. Luo, and H. Xiao, “Spatially continuous distributed fiber optic sensing using optical carrier based microwave interferometry,” *Optics Express*, Vol 22 ,No 15 ,pp 18757–18769 ,(2014)
- [7] E. Zhao, Y. Yuan, J. Yang, A. Zhou, and L. Yuan, “A novel multiplexed fiber optic deformation sensing scheme,” *Sensor Letters*, Vol 10 ,No 7 ,pp 1526–1528 ( 2012)
- [8] A. Yan, S. Li, Z. Peng, R. Zou, P. Ohodnicki, P. Lu, *et al.*, “Multi-point fiber optic sensors for real-time monitoring of the temperature distribution on transformer cores,” *SPIE*, 10639: 1063912 ,( 2018)
- [9] Z. Qu, S. Guo, C. Hou, J. Yang, and L. Yuan, “Real-time self-calibration PGC-Arctan demodulation algorithm in fiber-optic interferometric sensors,” *Optics Express*, Vol 27 ,No16 ,pp23593–23609, ( 2019)
- [10] S. Li, G. Lu, C. Lai, Y. Huang, and Y. En, “Optical-path difference on-line measurement of multiplexing fiber-optic interferometric sensors using TDM and WDM by improved opticalfrequency- domain reflectometry,” *SPIE*, 11340: 113400N (2019)

- [11] M. Wang, Y. Yang, S. Huang, J. Wu, K. Zhao, Y. Li, *et al.*, “Multiplexable high-temperature stable and low-loss intrinsic Fabry-Perot in-fiber sensors through nanograting engineering,” *Optics Express*, Vol 28, No 14 , pp20225–20235 (2020)
- [12] M. Ming and K. Liu, “Principles and Applications of Optical Communication”, McGraw –Hill, (1996).
- [13] T. Zhu, D. Wu, M. Liu and D. Duan, “In-Line Fiber Optic Interferometric Sensors in Single-Mode Fibers”, *Sensors*, Vol.12, pp.10430-49 (2012).
- [14] M. Bass. and E .Van Stryland, “Fiber Optics Handbook, Fiber, Devices, and Systems for Optical Communications”, optical society of America, McGraw –Hill, (2002).
- [15] B. H. Lee, Y. H. Kim , K. S. Park, J. B. Eom, M. J. Kim , B. S. Rho, and H. Y. Choi, "Interferometric Fiber Optic Sensors", *Sensors*, review, 12,pp. 2467-86, (2012).
- [16] ] Richard De La Rue , Hans Peter Herzig ,Martina Gerken," BIOLOGICAL AND MEDICAL PHYSICS ,BIOMEDICAL ENGINEERING " AG 2020
- [17] A. Yariv and P. Yeh, “Photonics: optical electronics in modern communications”, no. November. (2007)
- [18] Ramirez, J.C.; Lechuga, L.M.; Gabrielli, L.H.; Hernandez-Figueroa, H.E , "Study of a low-cost trimodal polymer waveguide for interferometric optical biosensors" *Opt. Express*, Vol 23, pp11985–11994 , (2015)
- [19] K. Suzuki, T. Mizuno, M. Oguma, T. Shibata, H. Takahashi, Y. Hibino, and A. Himeno, *IEEE Photonics Technol. Lett.* ,vol 16, pp 1480 , (2004).
- [20] Dong, P. et al. Submilliwatt, ultrafast and broadband electro-optic silicon switches. *Opt. Express* Vol 18, pp 25225–25231 (2010).
- [21] Zhou, H. et al. Performance influence of carrier absorption to the Mach-Zehnder-Interference based silicon optical switches. *Opt. Express* Vol 17, pp 7043–7051 (2009).
- [22] John M. Senior, " Optical Fiber Communications Principles and Practice " Third edition ,(2008)
- [23] Dr Jerry Benson , " New Uses for Multimode Optical Fibers " *Materials World*, Vol. 5 no. 9 pg. 412 September (2001)

- [24] Dr. Thaira Zakaria Abbas , " Fiber Optics" , unit 1, (2011-2012)
- [25] A. R. Bahrapour, S. Tofighi, M. Bathaee and F. Farman “Optical Fiber Interferometers and Their Applications”, *Optics Communications*, Vol.41, No.22, pp.4460-4483, (2012).
- [26] T. Wei, Y. Han, H.-L. Tsai, and H. Xiao, “Miniaturized fiber inline Fabry-Perot interferometer fabricated with a femtosecond laser,” *Optics Letters* , vol. 33, no. 6, pp. 536–538, (2008).
- [27] D. Hunger, T. Steinmetz, Y. Colombe , C. Deutsch, T. W. Hänsch, and J. Reichel, “A fiber Fabry-Perot cavity with high finesse,” *New J. Phys.*, vol. 12, (2010).
- [28] Tao Wei,<sup>1</sup> Yukon Han,<sup>2</sup> Yanjun Li, <sup>1</sup> Hai-Lung Tsai,<sup>2</sup> and Hai Xiao<sup>1</sup>,” Temperature-insensitive miniaturized fiber inline Fabry-Perot interferometer for highly sensitive refractive index measurement” *Optical Society of America*.,Vol. 16, no. 8, (2008).
- [29] D. Hunger, T. Steinmetz, Y. Colombe , C. Deutsch, T. W. Hänsch, and J. Reichel, “A fiber Fabry-Perot cavity with high finesse,” *New J. Phys.*, vol. 12, (2010).
- [30] Y. J. Rao, “Recent progress in fiber-optic extrinsic Fabry-Perot Interferometric Sensors,” *Optical Fiber Technology*, Vol. 12, No. 3, pp.227-237, (2006).
- [31] L. Jaroszewicz, Z. Krajewski and P. Marc, “Fiber optic Sagnac interferometer as a sensor of physical quantities ,” *Proceedings of SPIE - The International Society for Optical Engineering*, Vol. 5502, pp. 390-393,(2004).
- [32] H. Y. Fu *et al.*, “Pressure sensor realized with polarization-maintaining photonic crystal fiber-based Sagnac interferometer,” *Appl. Opt.*, vol. 47, no. 15, p. 2835, (2008).
- [33] Ai Zhou\*, Yaxun Zhang, Yuanyuan Yang, Jun Yang, and Zhihai Liu , " Ultra-high Sensitive Temperature Sensor Based on Multimode Fiber Mach-Zehnder Interferometer " the international society for optical engineering , Vol 9157 , (2014)
- [34] Vanita Bhardwaj\*, Vinod Kumar Singh " Fabrication and characterization of cascaded tapered Mach-Zehnder interferometer for refractive index sensing" *Sensors and Actuators A* 244 (2016) 30–34
- [35] Lu, L., Zhou, L., Li, Z., Li, X. & Chen, J. Broadband  $4 \times 4$  non-blocking silicon electrooptic switches based on Mach–Zehnder interferometers. *IEEE Photonics Journal* 7, 1–8 (2015).
- [36] Lu, L. et al.  $16 \times 16$  non-blocking silicon optical switch based on electro-optic Mach-Zehnder interferometers. *Opt. Express*, Vol 24, pp9295–9307 (2016).

- [37] Toshio Watanabe, Kohei Tasaki, Tsutomu Nagayama, and Seiji Fukushima " Nested Mach-Zehnder Interferometer Optical Switch with Low Crosstalk ," scientific reports pp 17 - 20, (2019)
- [38] QiZhang Yuan and Xunli Feng ," Three-path interference of a photon and reexamination of the nested Mach-Zehnder interferometer "PHYSICAL REVIEW A 99, 053805 (2019)
- [39] Zeqin Lu<sup>1</sup>, Dritan Celo<sup>2</sup>, Hamid Mehrvar<sup>2</sup>, Eric Bernier<sup>2</sup> & Lukas Chrostowski<sup>1</sup> " High-performance silicon photonic tri-state switch based on balanced nested Mach-Zehnder Interferometer," scientific reports ,Vol 7,No 12244 ,(2017)
- [40] Amma, Yoshimichi, et al. "Fusion splice techniques for multicore fibers," Optical Fiber Technology, Vol. 35, , pp. 72-79 ,(2017)
- [41] Svetlana S. Aleshkina, Tatiana A. Kochergina, Vladimir V. Velmiskin, Konstantin K. Bobkov, Mikhail M. Bubnov, Mikhail V. Yashkov, Denis S. Lipatov, Mikhail Yu. Salganskii, Alexey N. Guryanov & Mikhail E. Likhachev "High-order mode suppression in double-clad optical fibers by adding absorbing inclusions "Scientific Reports ,vol10, No7174 ,(2020)
- [42] K. Okamoto, "Fundamentals of optical waveguides" ,academic press,(2000).
- [43]H. Cherin, "Introduction to optical fibers", McGraw-Hill, 2nd Edition (1985).
- [44] T. Okoshi, "Optical Fibers", Elsevier, (2012).
- [45] A.E. Willner, Y.W. Song ,J. Mcgeehan and Z.Pan, "Dispersion Management", Elsevier, Vol., pp. 353-365,(2005).
- [46] K.S. Shuraavi and A. Fairouz ,"Optical Fiber - Dispersion, Construction, Application, Technology, Future",(2016).
- [47] P. Shanmugapriya and R. Raveena, "Analysis of Various Types of Fiber Dispersion for Fiber Optical Communication", International Conference on Smart Structures and Systems,pp.1-5,(2020).
- [48] M. Kyselák, P. Dorociak and M. Filka, "The Optical Modulation Format Impact on Polarization Mode Dispersion", Journal of Computer Science and Network Security, VOL.8 ,No.5, (2008).

- [49] J. P. Gordon, H. Kogelnik, "PMD fundamentals: Polarization mode dispersion in optical fibers", Proceedings of the National Academy of Sciences, Vol. 97, No.9, pp. 4541-4550,(2000).
- [50] Antonio Mecozzi,,Cristian Antonelli, and Mark Shtaif , " Nonlinear propagation in multi-mode fibers in the strong coupling regime" Optical Society of America , optics express ,Vol. 20, No. 11 ,(2012).
- [51] Paul L. Kelly, Ivan Kaminow, Govind P. Agrawal , "Optics and Photonics , Applications of Nonlinear Fiber Optics ", (2001)
- [52] Lecheng Li ,Li Xiaa, Zhenhai Xiea, Liangning Haoa, Binbin Shuaia, Deming Liua," In-line fiber Mach–Zehnder interferometer for simultaneous measurement of refractive index and temperature based on thinned fiber" Sensors and Actuators A, Vol 180,pp 19–24, (2012)
- [53] J. E. Antonio-Lopez,<sup>1</sup> A. Castillo-Guzman,<sup>2</sup> D. A. May-Arrijoa,<sup>3,\*</sup> R. Selvas-Aguilar,<sup>2</sup> and P. LiKamWa<sup>4</sup>;" Simultaneous measurement of refractive index and temperature using thinned fiber based Mach–Zehnder interferometer" Optics Communications , Vol 285 ,pp3945–3949 ,(2012)
- [54] D. A. Zheltikova; M. Scalova; A. M. Zhdtikov; M. J. Bloemer; M. N. Shneider; G. D. Aguanno; and R. B. Milles, "Switching intense Laser pulses Guided by Kerr-Effect-Modified Modes Of a Hollow –core Photonic crystal Fiber", Physical Review E71, 2005.
- [55] Xiaoliang Wang, Daru Chen, Haitao Li, Gaofeng Feng, Junyong Yang," In-Line Mach-Zehnder Interferometric Sensor Based on a Seven-Core Optical Fiber" IEEE Sensors Journal , Volume: 17, Issue 1, pp 100 – 104 , ( 2017)
- [56] YI LIU, GUOQIANG WU, RENXI GAO, AND SHILIANG QU<sup>2</sup>," High-quality Mach–Zehnder interferometer based on a microcavity in single-multi-single mode fiber structure for refractive index sensing",Applied Optics, Vol. 56, No. 4 , ( 2017 )
- [57] Ayah Thabit Yahiya , MS.C Thesis " Investigation of Mechanical Effects on the Performance of Mach-Zehnder Interferometer Filters", Institute of Laser for Postgraduate Studies , Baghdad University,(2018).
- [58] XiaoliZhao <sup>a</sup> MingliDong<sup>b</sup>YuminZhang <sup>a</sup> FeiLuo<sup>a</sup>LianqingZhu , " Simultaneous measurement of strain, temperature and refractive index based on a fiber Bragg grating and an in-line Mach–Zehnder interferometer" Optics Communications Volume 435, , Pages 61-67 ,15 March (2019)

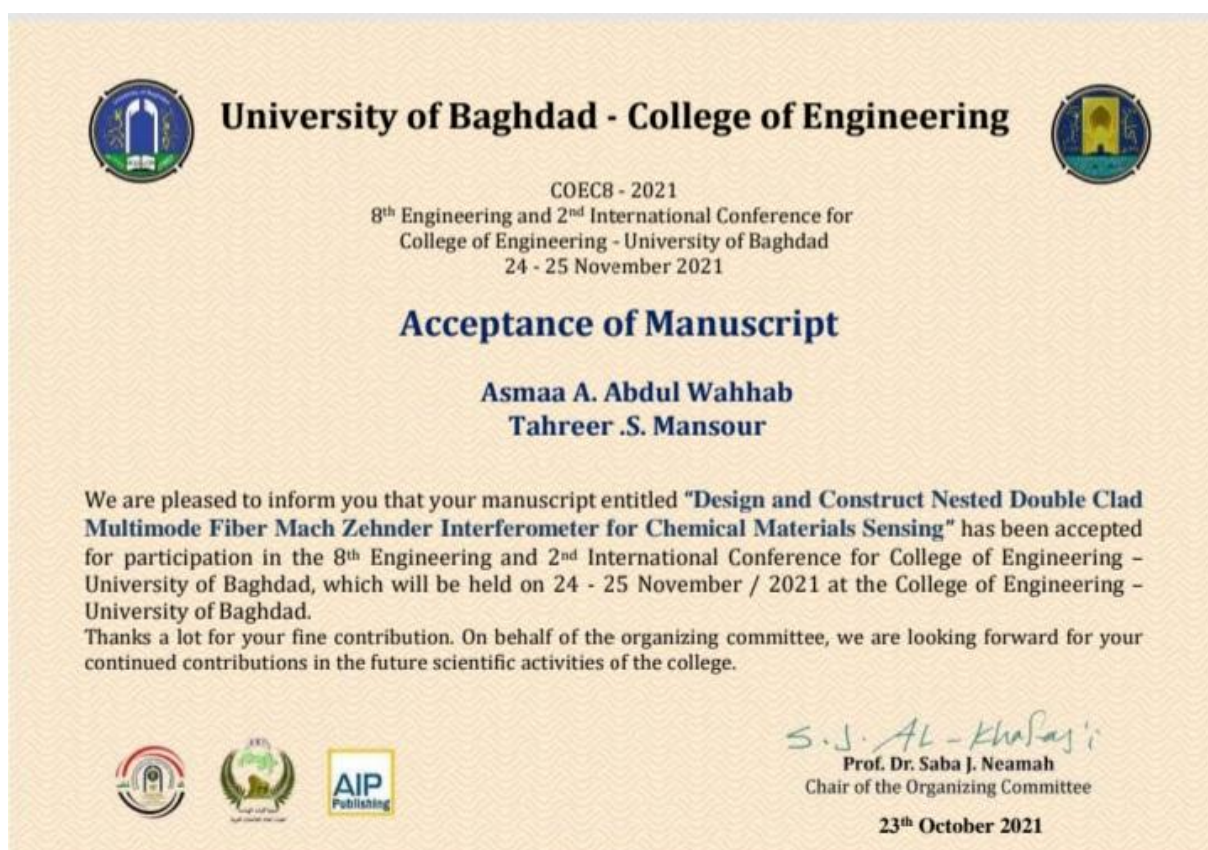
- [59] Yufei Cheng; Wenhua Zhu; Rongxin Tong; Manli Hu; Tingting Gang," A Novel Optical Fiber Mach–Zehnder Interferometer Based on the Calcium Alginate Hydrogel Film for Humidity Sensing" *IEEE Sensors Journal* ,Volume: 20, Issue: 11, ( 2020)
- [60] W. Inart, and W. Asawamethapant, “The analysis of parameters related to fusion splicing loss of SMF-28 and MP980” *International Conference on Electrical Engineering/Electronics, Computer, Telecommunications and Information Technology IEEE Xplore* , Vol 8, No 614 , pp 1-4 , (2012).
- [61] Ali Ahmed Dawood " Design and Implementation of In Line Fiber Pulse Compression using Photonic Crystal Fiber " Thesis Submitted to the Institute of Laser for Postgraduate Studies, University of Baghdad ,(2020)
- [62] Kent F. Palmer and Dudley Williams , " Optical properties of water in the near infrared" *Journal of the Optical Society of America* , Vol. 64, [Issue 8](#), pp. 1107-1110 , (1974)
- [63] H. A. Razak, H. Haroon, P. S. Menon, S. Shaari and N. Arsad, “Design and optimization of a Mach-Zehnder Interferometer (MZI) for optical modulators” *IEEE International Conference on Semiconductor Electronics (ICSE2014)*,Vol 24,No 12 , pp.301-304,(2014).
- [64] Yuxuan Jiang, Yating Yi, Gilberto Brambilla, and Pengfei Wang , " High-sensitivity, fast-response ethanol gas optical sensor based on a dual microfiber coupler structure with the Vernier effect" *Optics Letters*, Vol. 46 , pp. 1558-1561 , (2021)
- [65] Jessica E. Q. Bautista, Manoel L. da Silva-Neto, Cecilia L. A. V. Campos, Melissa Maldonado, Cid B. de Araújo, and Anderson S. L. Gomes." Thermal and non-thermal intensity dependent optical nonlinearities in ethanol at 800 nm, 1480 nm, and 1560 nm", *Journal of the Optical Society of America B* , Vol. 38, , pp 1104-1111 , (2021) .
- [66] N.Zahmouli<sup>ad</sup> ,M.Hjiri<sup>bd</sup> ,S.G.Leonardi<sup>a</sup> ,L.El Mir<sup>d</sup> ,G.Neri ,D.Iannazzo<sup>a</sup>C.Espro<sup>a</sup> ,M.S.Aida<sup>bc</sup>," High performance Gd-doped  $\gamma$ -Fe<sub>2</sub>O<sub>3</sub> based acetone sensor" *Materials Science in Semiconductor Processing* , Volume 116, No 105 ,pp 154 ,(2020)
- [67] jinbao xia, feng zhu,alexandre a. kolomenskii, james bounds, sasa zhang,mahmood amani, liam j. fernyhough, and hans a. schuessler , " sensitive acetone detection with a mid-ir inter band cascade laser and wavelength modulation spectroscopy" *osa continuum* ,vol. 2, No. 3 ,PP 640 , (2019)



# **PUBLICATIONS**

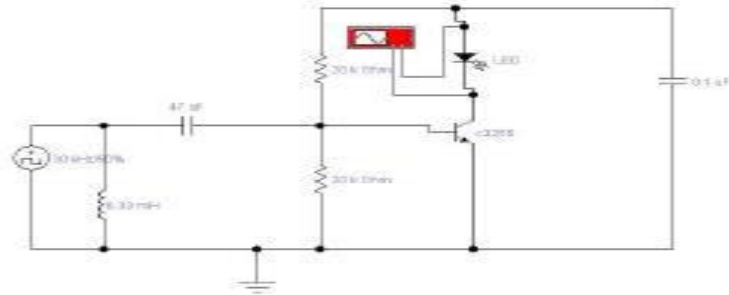
## List of Publications

- 1- **Asmaa. A. Abdul Wahhab and Tahreer S. Mansour** ," Design and Analysis of BIMD Double Clad MMF -MZI Using Optiwave Simulation " Iraqi journal of laser ,Vol 20 ,pp1-5 ,(2021)
- 2- **Asmaa. A. Abdul Wahhab** , Yousif I. Hammadi, Tahreer .S. Mansour ," Design and Construct Nested Double Clad Multimode Fiber MZI (DC-MMF –NMZI) for Pregnancy Test"  
Journal of Mechanical Engineering Research and Developments Vol. 44, No. 10, pp. 12-22 ,(2021)
- 3-**Asmaa. A. Abdul Wahhab** ,and Tahreer .S. Mansour ," Design and construct Nested Double Clad Multimode Fiber Mach Zehnder Interferometer using pulsed laser for chemical materials sensing ", 'AIP conference Reecedings of COEC-8 –final acceptance (2021)

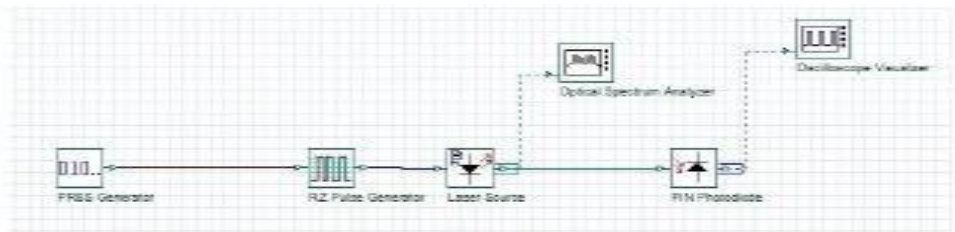


# Appendices

# Appendix A



Schematic Diagram of Electronic Chopping circuit



simulation by Opti-system of Electronic Chopping circuit

**Specifications**

Parameter	Value	Unit
Central wavelength	1546.74	nm
Pulse duration	10	ns
FWHM	286	pm
Pulse repetition rate	30	kHz
Duty-cycle	90%	—
Energy	0.0123	nJ
Power	1229.271	µW
Voltage	2	mV
Frequency	30	kHz

# Appendix B

B1

## EDFA



[PÁGINA DE INICIO](#) [PRODUCTOS](#) [SOLUCIÓN](#) [APOYO](#) [NOTICIAS](#) [SOBRE NOSOTROS](#) [CONTÁCTENOS](#)


Item*	values
Output Power (dBm)	15 16 17 18 19 20 21 22 23 24
Input power (dBm)	-5~+10
Wavelength (nm)	1540~1560
Output power stability (dB)	<±0.2
Bias oscillation sensitivity (dB)	<0.2
Bias oscillation dispersion (PS)	<0.5
Optical return loss (dB)	>40
Fiber connector	FC/APC or SC/APC
Noise ratio (dB)	<5.0(0dBm optical input)
connector	RS232 or RS485、RJ45
Power loss (W)	50
Working Voltage (V)	220V

# Appendix C

TELEWEAVER

[PLC Splitter](#)
[FBT Splitter](#)
[Wiki & Tutorial](#)
[Factory](#)
[Contact](#)

[Home](#) > [FBT Fiber Splitters](#) > [1×3 Single Mode Fibre Optic Splitter ABS Box FBT Fused Type Optical Coupler FC/APC Connector](#)



### 1×3 Single Mode Fibre Optic Splitter ABS Box FBT Fused Type Optical Coupler FC/APC Connector

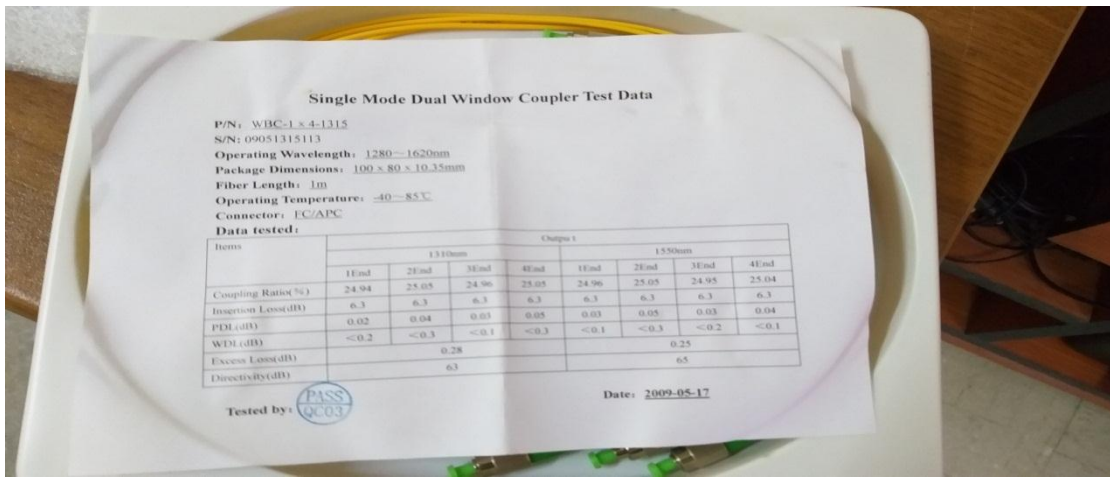
- Free 1×3 Single Mode Fibre Optic Splitter Sample
- 1310/1550nm or 1310/1490/1550nm
- SC FC LC ST or other Customized Connectors
- Low Insertion Loss & High Return Loss
- Plastic Module Package for Safe Protection
- Different Fiber Cable Diameters Supplied
- Detailed Test Report Label

Teleweaver P/N: #FBT13-A-SC-U  
Product ID: #1597

\$7.26/pcs

[Send Inquiry Now](#)

Free sample(s) will be sent in 1-3 days usually.



shenzhen new vision optical communication Co.,LTD

OVERVIEW
CUSTOMER REVIEWS (0)
SPECIFICATIONS
Report Item

**1\*4,Single Mode,Dual Window,1310/1550,FBT Fiber Fused Optic Coupler,ABS Box,100\*80\*10,2.0mm,25/25/25/25,L:1M,SC/APC**

1.Type: 1xN, 2xN  
2.FTTx, xPON, LAN  
3.ABS box, mini module  
4.ISO 9001  
1x2 fiber optic plc splitter  
Type: 1xN, 2xN  
For FTTx, xPON, LAN  
ABS box, mini module, break-out, rack, wall, box  
ISO 9001

**1\*4,Single Mode,Dual Window,1310/1550,FBT Fiber Fused Optic Coupler,ABS Box,100\*80\*10,2.0mm,25/25/25/25,L:1M,SC/APC**

**Description:**plc splitter are based on the Planar Waveguide Technology. They provide a cost effective and space saving networking solution. They are key components in FTTX networks and are responsible to distribute the signal from central office to numbers of premises. They have very wide range of operating wavelength from 1260nm to 1620nm. With it's compact size, these splitters can be utilized in in-ground and aerial pedestals as well as rack mount systems.

- 1.Low Insertion loss
- 2.Wide Operating Wavelength
- 3.Compact Size
- 4.Excellent Environmental & Mechanical Stability

Specifications

# Appendix D

**TELEFLY** Professional Manufacturer Since 2004

ISO 9001 SGS [www.telefly.cn](http://www.telefly.cn) RoHS Compliant TLC

## Appendix E

### OSA (FBGA) properties

Specifications	Unit	Data
Standard Wavelength Ranges*	Standard: 1525-1565 Extended: 1510-1590	Nm
Wavelength Repeatability	+2	Pm
Wavelength Readout Resolution	1	Pm
Minimum Detectable Wavelength Change	+ 1	Pm
Frequency response time (typ.)	Standard: ~5 Hz (RS232/USB1.1) Fast: ~5 kHz (USB2.0)	
IRS - Internal Reference Source	Integrated	Yes
Channel Input Power Range	-60 to -20 or specify	dBm
Power Resolution	0.1	Db
Size	Standard: 113.5 x 84 x 47.5 Thin: 148 x 142 x 29.1	mm <sup>3</sup>
Interface	RS232 or USB (Fast board USB only)	
Operating Temperature	-5 to +70	C°



# Appendix F

# 300

NETWORK TESTING

**POWER METER**

FPM-300



- Highly accurate unit offering 10 calibrated wavelengths and reference values
- Power autonomy of 300 hours
- Three-year warranty and recommended calibration interval, for dramatically reduced cost of ownership
- Ergonomic, eye-catching handheld package

The FPM-300 Power Meter is part of EXFO's new line of handheld units, which includes the FLS-300 Light Source and the FOT-300 Optical Loss Test Set.

#### **Auto-Wavelength Recognition**

The FLS-300 or FOT-300 units can transmit with a wavelength-identification digital encrypted protocol, enabling the FPM-300 Power Meter to automatically use the proper calibration parameters. This feature reduces the need for communication between the two technicians and decreases the potential for error.

#### **Distant Referencing**

Signal encrypting can also give the receiving end information on the power to be used as reference, helping ensure efficient referencing, even when the two units are far apart.

#### **No Offset Nulling**

Thanks to its unique design, the FPM-300 Power Meter reduces measurement time in typical measurement situations, as the need for an offset nulling is eliminated.

#### **FTTx Ready**

EXFO's FPM-300 allows for the testing of passive optical networks (PONs) at 1310 nm, 1490 nm and 1550 nm, the three wavelengths recommended by the ITU-T (G.983.3) for PONs.



# Appendix G

G1

## Ethanol chemical properties.

<b><u>Chemical formula</u></b>	<b>C<sub>2</sub>H<sub>6</sub>O</b>
<b><u>Molar mass</u></b>	46.069 g·mol <sup>-1</sup>
<b><u>Appearance</u></b>	Colourless liquid
<b><u>Odor</u></b>	Methanol-like <sup>[2]</sup>
<b><u>Density</u></b>	0.78945 g/cm <sup>3</sup> (at 20 °C) <sup>[3]</sup>
<b><u>Melting point</u></b>	-114.14 ± 0.03 <sup>[3]</sup> °C (-173.45 ± 0.05 °F; 159.01 ± 0.03 K)
<b><u>Boiling point</u></b>	78.23 ± 0.09 <sup>[3]</sup> °C (172.81 ± 0.16 °F; 351.38 ± 0.09 K)
<b><u>Solubility in water</u></b>	<u>Miscible</u>
<b><u>log P</u></b>	-0.18
<b><u>Vapor pressure</u></b>	5.95 kPa (at 20 °C)
<b><u>Acidity (pK<sub>a</sub>)</u></b>	15.9 (H <sub>2</sub> O), 29.8 (DMSO) <sup>[4][5]</sup>
<b><u>Magnetic susceptibility (χ)</u></b>	-33.60·10 <sup>-6</sup> cm <sup>3</sup> /mol
<b><u>Refractive index (n<sub>D</sub>)</u></b>	1.3611 <sup>[3]</sup>
<b><u>Viscosity</u></b>	1.2 mPa·s (at 20 °C), 1.074 mPa·s (at 25 °C) <sup>[6]</sup>
<b><u>Dipole moment</u></b>	1.69 D <sup>[7]</sup>

# Appendix H

## Acetone chemical properties [65]

Property	Value	Unit		Value	Unit		Value	Unit		Value	Unit
<b>Acidity (pKa1)</b>	20										
<a href="#">Autoignition temperature</a>	738	K		465	°C		869	°F			
<b>Boiling Point</b>	329.2	K		56.08	°C		132.9	°F			
<b>Critical density</b>	4.70	mol/dm <sup>3</sup>		273	kg/m <sup>3</sup>		0.530	slug/ft <sup>3</sup>		17.0	lb/ft <sup>3</sup>
<b>Critical pressure</b>	4.69	MPa=MN/m <sup>2</sup>		46.9	bar		46.3	atm		681	psi=lb/in <sup>2</sup>
<a href="#">Critical temperature</a>	508.1	K		235.0	°C		454.9	°F			
<b>Critical volume</b>	213	cm <sup>3</sup> /mol		0.00366	m <sup>3</sup> /kg		1.89	ft <sup>3</sup> /slug		0.0587	ft <sup>3</sup> /lb
<a href="#">Density</a>	13507	mol/m <sup>3</sup>		784.5	kg/m <sup>3</sup>		1.522	slug/ft <sup>3</sup>		48.97	lb/ft <sup>3</sup>
<b>Flammable, gas and liquid</b>	yes										
<a href="#">Flash point</a>	256	K		-17	°C		1	°F			
<a href="#">Gas constant, individual</a> – R	143.2	J/kg K		0.03977	Wh/(kg K)		856.1	[ft lbf/slug °R]		26.61	[ft lbf/lb °R]
<a href="#">Gibbs free energy of formation (gas)</a>	-153	kJ/mol		-2634	kJ/kg		-1133	Btu/lb			
<a href="#">Heat (enthalpy) of combustion (gas)</a>	-1821	kJ/mol		-31354	kJ/kg		-13.5	Btu/lb			
<b>Heat (enthalpy) of combustion (liquid)</b>	-1789	kJ/mol		-30803	kJ/kg		-13.2	Btu/lb			
<a href="#">Heat (enthalpy) of formation (gas)</a>	- 218.0	kJ/mol		-3753	kJ/kg		-1614	Btu/lb			
<b>Heat (enthalpy) of formation (liquid)</b>	-249	kJ/mol		-4287	kJ/kg		-1843	Btu/lb			

# Appendix I

## Digital PAL-BX/RI refract meter



PAL-BX/RI features a dual scale. Brix (wide range 0.0-93.0%) and Refractive Index (resolution 0.0001).

Digital Hand-held "Pocket" Dual Scale Refractometer

# PAL-BX/RI

Cat.No.3852

### Measurement Method



1. Place the sample onto the prism surface.



2. Press the START key.



3. The measurement value will be displayed in 3 seconds.

4. Press the START key for 2 seconds while the Brix (%) is indicated, to display the Refractive Index and temperature. Press the START key (one time) to return to the Brix (%) scale.

#### Example of display

Display of the measurement value "1.3425" and "20°C".



The measurement value for Refractive Index will scroll from right to left.



### Features

- Requires only a few drops of sample
- Measurement in 3 seconds
- Ergonomically designed for easy, one-handed operation
- Light & Compact, 100g
- Designed with a strap holder option
- Highly water resistant (IP65)
- Convenient storage case
- Battery power indicator

### Specifications

Measurement range	Brix : 0.0 to 93.0% (9.0 to 99.9°C) Refractive Index (RI) : 1.3306 to 1.5284 (5.0 to 45.0°C)
Resolution	Brix : 0.1%    Refractive Index : 0.0001    Temperature : 0.1°C
Measurement accuracy (Automatic Temperature Compensation)	Brix : ±0.1%    Refractive Index : ±0.0003 (Water at 20°C) Temperature : ±1°C
Measurement temperature	10 to 100°C (Brix only)
Ambient temperature	10 to 40°C
Power supply	AAA alkaline battery × 2
Battery life	Approx. 11,000 measurements (using new alkaline batteries)
International Protection Class	IP65 Water resistant
Dimensions and weight	55(W) × 31(D) × 109(H)mm, 100g (main unit only)

\* The displayed measurement value for Refractive Index is not temperature compensated. The reading is the Refractive Index of the sample at the temperature displayed.

All ATAGO refractometers are designed and manufactured in Japan.



ATAGO products comply with HACCP, GMP and GLP system standards.



\* Specifications and appearance are subject to change without notice.

Find Quality Products Online at:

[www.GlobalTestSupply.com](http://www.GlobalTestSupply.com)

[sales@GlobalTestSupply.com](mailto:sales@GlobalTestSupply.com)

1207K Printed in Japan

## الخلاصة

سرعة الكشف هي واحدة من اهم العمليات التي يمكن الحصول عليها من خلال قيمة ال (FWHM<sub>spatially</sub>). ولذلك لاستخدامها في انظمة وتطبيقات الاتصالات المتقدمة نظرا لما توفره من سرعة بيانات عالية .

في هذا العمل يستخدم مقياس التداخل الضوئي كنظام كشف سريع وقابل للاستخدام عدة مرات والذي تم تصميمه باستخدام الليف الضوئي متعدد الانماط تم نفعه لتخديش طبقة ال clad نوع ماخ زندر وتم اعتماد طريقة ربط ال nested لكي تعمل كشبكة تحسس ضوئية .

تم استخدام برنامجين للمحاكاة لتنفيذ نظام الكشف نظريا . الليف الضوئي متعدد الانماط والذي يعمل كراس متحسس تم ، تصميمه بثلاثة اسماك مختلفة 110 مايكرو ميتر ، 100 مايكروميتر و 90 مايكرو ميتر وثلاث معمل انكسار مختلفة والتي تمثل بدورها القشرة المحيطة براس التحسس وذلك باستخدام برنامج المحاكاة Opt grating Version 4.2.2. تم قياس نتائج تطبيق باستخدام برنامج المحاكاة Version 15 وكانت اعلى قيمة لل FWHM هي 106 بيكوميتر عند سمك الليف الضوئي 90 مايكروميتر.

كفاءة اداء نظام الكشف تحققت عمليا باستخدام مصدر ليزر يعمل ضمن نطاق ال C-band بطول موجي 1546.74 نانوميتر وبعرض نبضة 10 نانو ثانية بطاقة مقدارها 1.23 ميلي واط .النظام المصمم استخدم لكلا التطبيقين الكيميائي والبيولوجي .اولا بالنسبة للتطبيق الكيميائي تم استخدام السوائل العضوية (C<sub>2</sub> H<sub>5</sub> OH)and (CH<sub>3</sub>-CO-CH<sub>3</sub>) بالإضافة الى الماء المقطر حيث ان قيمة ال FWHM للماء المقطر هي 196 بيكو ميتر عند سمك الليف الضوئي 112.9 مايكروميتر وللايثانول هي 292 بيكوميتر عند سمك الليف الضوئي 118.7 مايكروميتر وللأسيتون هي 365 بيكوميتر عند سمك الليف الضوئي 112.9 مايكروميتر .اما للتطبيقات البيولوجية تم استخدام ثلاث عينات من ادرار الحوامل مقارنة مع عينة ادرار لغير الحامل وذلك للتحقق من قابلية اداء نظام الكشف (اختبار حمل) .كانت قيمة FWHM هي 243 بيكوميتر لعينة الغير حامل عند سمك الليف الضوئي 112.9 مايكروميتر ، 147 بيكوميتر لعينة الحامل الاولى عند سمك الليف الضوئي 72.5 مايكروميتر ، 317 بيكو ميتر لعينة الحامل الثانية عند سمك الليف الضوئي 112.9 مايكروميتر.

من خلال النتائج التي تم قياسها نستنتج ان سرعة الكشف وجدت عند حالة ربط ال nested حيث ان اقل قيمة ل FWHM هي 209 بيكوميتر عند الطول الموجي 1547.2 نانوميتر وقدرة مقدارها 66.7 مايكرو واط .اما للتطبيقات البيولوجية اسرع FWHM تم كشفها 333 بيكوميتر عند طول موجي 1546.85 نانوميتر وقدرة 7.66 مايكرو واط عند عينة الحامل الثالثة .



وزارة التعليم العالي والبحث العلمي

جامعة بغداد

معهد الليزر للدراسات العليا

**تصميم وتنفيذ مقياس التداخل ماخ زندر باستعمال الليف الضوئي ثنائي القشرة متعدد  
الانماط للاستشعار الشبكي**

رسالة مقدمة الى

**معهد الليزر للدراسات العليا / جامعة بغداد / لاستكمال متطلبات نيل شهادة ماجستير علوم  
في الليزر / الهندسة الالكترونية والاتصالات**

من قبل

**اسماء انعام عبدالوهاب**

بكالوريوس الهندسة الالكترونية والاتصالات - ٢٠١٣

بإشراف

**الأستاذ المساعد الدكتورة تحرير صفاء منصور**

٢٠٢١ م

١٤٤٣ هـ